AD-A094 469 INDIANA UNIV AT BLOOMINGTON DEPT OF CHEMISTRY F/G 7/4
SATURATION OF ENERGY LEVELS IN ANALYTICAL ATOMIC FLUORESCENCE S--ETC(U)
JAN 81 D R OLIVARES, G M HIEFTJE N00014-76-C-0838
UNCLASSIFIED TR-34 NL

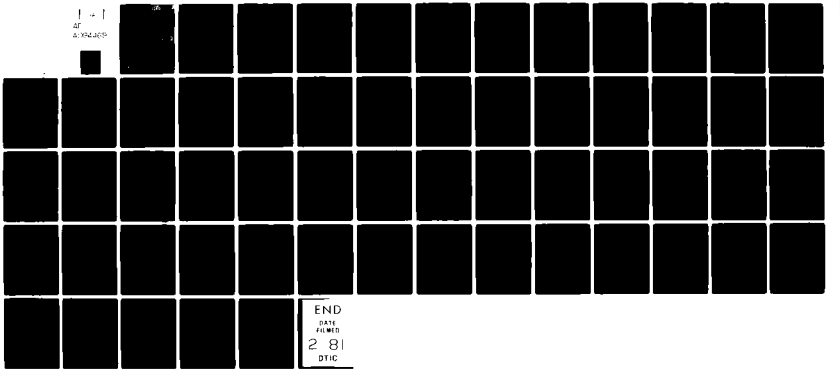

END
DATE FILMED
2 81
DTIC

UNCLASSIFIED

SECURITY CLASSIFICATION OF THIS PAGE (When Data Entered)

LEVEL II AD A094469

REPORT DOCUMENTATION PAGE

READ INSTRUCTIONS BEFORE COMPLETING FORM

1. REPORT NUMBER: THIRTY-FOUR	2. GOVT ACCESSION NO. AD-A094469
3. RECIPIENT'S CATALOG NUMBER	
4. TITLE (and Subtitle): Saturation of Energy Levels in Analytical Atomic Fluorescence Spectrometry. II. Experimental.	5. TYPE OF REPORT & PERIOD COVERED: Interim Technical Report
	6. PERFORMING ORG. REPORT NUMBER: 42
7. AUTHOR(s): Dorys Rojas de Olivares and Gary M. Hieftje	8. CONTRACT OR GRANT NUMBER(s): N14-76-C-0838
9. PERFORMING ORGANIZATION NAME AND ADDRESS: Department of Chemistry, Indiana University, Bloomington, IN 47405	10. PROGRAM ELEMENT, PROJECT, TASK AREA & WORK UNIT NUMBERS: NR 51-622
11. CONTROLLING OFFICE NAME AND ADDRESS: Office of Naval Research, Washington, D.C.	12. REPORT DATE: January 30, 1981
	13. NUMBER OF PAGES: 54
14. MONITORING AGENCY NAME & ADDRESS (if different from Controlling Office)	15. SECURITY CLASS. (of this report): UNCLASSIFIED
	15a. DECLASSIFICATION/DOWNGRADING SCHEDULE

16. DISTRIBUTION STATEMENT (of this Report)

Approved for public release; distribution unlimited

DTIC ELECTE FEB 0 3 1981 S D E

17. DISTRIBUTION STATEMENT (of the abstract entered in Block 20, if different from Report)

18. SUPPLEMENTARY NOTES

Prepared for publication in SPECTROCHIMICA ACTA, PART B

19. KEY WORDS (Continue on reverse side if necessary and identify by block number)

atomic fluorescence
flame spectrometry
laser-induced fluorescence
energy-level saturation
saturation spectroscopy

20. ABSTRACT (Continue on reverse side if necessary and identify by block number)

~~In part I of this investigation~~, a theoretical model was proposed to describe the saturation of atomic energy levels under conditions of intense but brief irradiation by a suitable exictation source. The experimental verification of that model is presented herein. In this study, the effects on dye laser-induced saturation of analyte concentration, flame composition and atomic properties of the elements were all examined and quantitated in terms of a measurable parameter, the saturation spectral power density

DD FORM 1 JAN 73 1473 EDITION OF 1 NOV 65 IS OBSOLETE S/N 0102-014-6601

UNCLASSIFIED

SECURITY CLASSIFICATION OF THIS PAGE (When Data Entered)

81 2 02 195

AD A094469

DTIC FILE COPY

20. Abstract (continued)

(SSPD). The results of those studies reveal that SSPD is relatively independent of analyte concentration and flame composition but is a strong function of the nature of each particular atomic transition employed. Moreover, because of strong quenching in most analytical flames, a simple steady-state model for saturation applies even for brief, 5.6 ns. pulses from a nitrogen-laser pumped dye laser. Most importantly, it is shown that reliable values for the SSPD can be obtained only through careful experimental design; considerations important in such measurements are therefore carefully detailed.

OFFICE OF NAVAL RESEARCH

Contract N14-76-C-0838

Task No. NR 051-622

TECHNICAL REPORT NO. 34

SATURATION OF ENERGY LEVELS IN ANALYTICAL ATOMIC FLUORESCENCE SPECTROMETRY

II. EXPERIMENTAL

by

Dorys Rojas de Olivares and Gary M. Hieftje

Prepared for Publication

in

SPECTROCHIMICA ACTA, PART B

Indiana University

Department of Chemistry

Bloomington, Indiana 47405

January 30, 1981

INTRODUCTION

Among the different techniques which have been developed for trace metal analysis, atomic emission, absorption and fluorescence spectrometry are the most widely used. Of these techniques, atomic fluorescence spectrometry (AFS) is the most recently developed and offers the combined advantages of high specificity for the determination of individual elements, high sensitivity, simplicity and applicability to multielement analysis.

AFS involves the excitation of isolated atoms by a suitable primary source and the subsequent detection of the radiation which is emitted by the fraction of excited atoms which deactivates radiatively. Although fundamental studies in the AFS of metal vapors were performed even as early as 1900 (1, 2), it was not until 1964 that the use of AFS as an analytical technique was reported (3-5). Since that time, most of the effort in analytical AFS has been devoted to optimization and development of high efficiency atomizers (6-8) and high radiance excitation sources (9-11). These areas have received greatest attention because of the linear dependence of the detected fluorescence signal on the concentration of neutral analyte atoms and (at low incident radiant flux) on the spectral irradiance of the excitation source.

With the development of very high spectral radiance sources (such as pulsed tunable dye lasers), AFS has become a potentially even more powerful analytical technique and the study of fundamental processes in atomic spectroscopy has been made easier. Several previous studies dealing with laser-excited AFS have revealed that a saturation of atomic energy levels can be produced which limits the maximum fluorescence signal achievable at any

given analyte concentration. This saturation or "bleaching" effect of atomic energy levels, besides limiting the attainable sensitivity of laser-excited AFS, provides several important practical features. Most important of these features are an increase in the range of linearity of analytical working curves, freedom of the fluorescence signal from excited-state quenching effects in the atom environment, and freedom from power instabilities of the excitation source (laser) (12-25).

When a high spectral radiance source such as a laser is employed in AFS, the rates of population and depopulation of the excited state become radiationally controlled. When such stimulated processes dominate, any other activation (chemical or thermal) or deactivation (quenching, spontaneous radiation) pathways do not strongly affect the equilibrium population of the excited state. Consequently, the magnitude of the excited state population and of the detected (spontaneous) fluorescence become nearly constant.

It might at first seem that stimulated emission, being the main route of deactivation of a saturated energy level, would completely overwhelm the detection of the smaller but constant spontaneous fluorescence. However, the stimulated emission is by nature directed along the path of the exciting radiation and is not detected by a measuring system lying in any other direction. In contrast, spontaneous fluorescence is isotropic and will therefore be detectable at any angle.

In order to take full advantage of all the potentially useful features of laser-excited AFS, it is necessary to characterize the fluorescence radiation emitted under conditions of high incident source radiance. Furthermore, a thorough understanding of the saturation process should enable

an assessment of the importance of fundamental processes such as quenching and nonquenching collisions in the atom cell. In characterizing the fluorescence radiation emitted under saturation conditions, it becomes important to know the minimum incident power density which would be necessary to achieve the saturation.

Previous investigations into the saturation of atomic energy levels at high spectral irradiance has predicted little, if any, effect of the quenching characteristics of the atom environment on the saturation power density (12-25). Also, all the theoretical models proposed to explain the saturation effect have assumed that steady-state conditions prevail in the population of the excited level, an assumption which is valid only if the duration of the excitation pulse is much longer than the fluorescence lifetime of the transition being studied. Because typical values of spontaneous atomic fluorescence lifetimes are 1-20 ns, such steady-state conditions do not prevail in unquenched atomic systems excited by a short-pulsed nitrogen-pumped tunable dye laser (typical pulse width: 1-10 ns), although they are approached when longer duration sources are used. One latter such source is the flash-lamp-pumped tunable dye laser (typical pulse width: 1-10 μs).

In the present study, experimental and predicted values of saturation power density were determined and their dependence on atom-environment and on the spectral and spatial characteristics of the irradiance source was ascertained. The study was comprised and is being reported in two parts.

In part I of the study (26) a theoretical model was proposed to describe the saturation of atomic energy levels by a radiation pulse of variable duration and power density. The model enables the prediction of saturation power densities of transitions involving two and three atomic energy levels

under both steady state (continuous-wave) and non-steady-state (transient) irradiation. In that report, values of predicted spectral power density necessary to saturate several specific atomic transitions were presented and the dependence of saturation spectral power density on the excitation pulse duration was illustrated.

In the present paper, experimentally determined values of saturation spectral power density for a series of atomic transitions will be reported and compared to values predicted by the model developed in part I (26). The saturation spectral power density (SSPD) is that level of incident source spectral power density ($W/cm^2 \cdot Hz$ or $W/cm^2 \cdot nm$) required to produce fifty percent of the "saturated" fluorescence radiance level; consequently, the SSPD was experimentally determined for each transition by plotting a measured spontaneous fluorescence signal against the effective spectral irradiance produced by the excitation source (laser).

It will be shown that experimental conditions necessary for obtaining accurate values of SSPD are critical; these conditions will be described and the influence of experimental parameters such as atom concentration, atom environment, temporal gate-width of the detector and type of transition will be illustrated. Flames having different composition and temperature were used as the atom-cell during SSPD measurements. Experimental values of SSPD obtained with these measurements will be compared with those predicted by the model proposed in part I of this study; the resulting agreement enables useful conclusions to be drawn concerning the feasibility and practicability of employing saturated atomic fluorescence spectrometry for routine analysis.

EXPERIMENTAL MEASUREMENTS AND CONDITIONS

The following instrumentation was employed in these measurements: an excitation source consisting of a nitrogen-laser-pumped tunable dye laser whose beam has been rendered spatially homogeneous in the region of interest; a flame of controllable composition, used as an atom source and reservoir, a detection, signal processing, and read-out system, oriented at 90° with respect to the excitation source and which consists of a low-scattered-radiation monochromator, a fast photomultiplier, delay line, boxcar integrator and recorder; finally, a fast power-meter was used to measure the power of the laser beam at the flame position. Figure 1 shows a block diagram of these devices; their most important characteristics and their effects on the fluorescence measurements are discussed in the following section.

In order to obtain reliable fluorescence measurements, several requirements must be met. First, to maintain a uniformly illuminated flame volume for meaningful physical measurements, the diameter and power of the laser beam must be held constant or be known and its homogeneity assured. Second, scattering of source radiation should be minimized (27) by using a sample introduction and atom formation system which is highly efficient and generates few particulate species within the atom observation region. To avoid the distortions produced by pre- and post-filter effects in the fluorescence measurements, and to maximize the detected fluorescence signal, the flame shape and burner-top must be carefully chosen and designed. Finally, careful optical alignment between the laser beam, the flame and the monochromator must be maintained. The way in which these requirements were met is described in the following sections. For further details concerning the original components, the reader is referred to the Ph.D. thesis of one of the authors (28).

The tunable dye laser (UV-400, Molectron, Inc., Sunnyvale, CA) employed as a source was pumped by a nitrogen laser (UV-1000, Molectron, Inc., Sunnyvale, CA). Although sometimes erratic in its operation, this system was capable with constant attention of saturating many atomic transitions of interest.

To minimize scattering of the incident source radiation (27), an ultrasonic nebulizer (Tomorrow Enterprises, Portsmouth, OH) and a laminar, well characterized flame were used to generate atoms. The flame was supported on a laminar-flow burner of the Alkemade design (29,30). To provide an atomic population of relatively uniform temperature, a flowing argon shield surrounded the flame. This argon shield reduces air entrainment at the base of the flame which would otherwise change the temperature and composition at the edge of the flame and thereby produce a non-uniform distribution of atom concentrations and increase quenching by air constituents. Also, a 4 cm diameter quartz tube was used to surround the flame to protect it against laboratory air currents and to reduce multiplicative noise which would otherwise be carried through the detection and measurement system (31).

Because the Alkemade burner was not originally designed to handle large volumes of analytical solutions, it was modified to improve its coupling to the ultrasonic nebulizer. To avoid condensation of the nebulized solution, the distance between the nebulizer and the burner chamber was kept within 3 cm for the air-acetylene flame and 8 cm for the hotter flames such as oxygen-argon-acetylene.

Purified flame gases (acetylene from Linde Div., Union Carbide Corp., N.Y., all others from Matheson Co., Joliet, IL) were controlled by needle valves (Fine Metering Valves, Nupro, Cleveland, OH) and monitored by cali-

brated flowmeters (603 and 604), Matheson, East Rutherford, NJ). Oxidant and fuel gases were pre-mixed and stream-split before entering the burner; a small fraction of the pre-mixed gases was then used as a carrier for nebulized solutions. Optical gas flows (corrected to STP) for the different types of flames used in this study are shown in table 1. In all cases, the flame operates in a slightly fuel-rich condition, which has been found to promote atom formation efficiency and reduce errors in saturation caused by ionization (32).

The range of flame types shown in table 1 were employed to enable a study of the effects of flame composition, temperature and quantum efficiency on the characteristics of laser-excited AFS.

The detection system used in the present work consists of a filter/grating monochromator (model EU-700-77, McPherson Co., Acton, MA), and a 1P28 photomultiplier tube (RCA) operated at -950 volts. This monochromator has an assembly of eight filters which provide a preliminary stage of wavelength discrimination, serving to reduce higher-order diffracted radiation and detected stray light.

A dual-channel boxcar integrator (Models 162, 163, 164, Princeton Applied Research Co., Princeton, NJ) provided alternatively a time-resolved or time-integrated representation of the fluorescence signal, which were then recorded by suitable analog or digital devices. Also, the device automatically corrected for background radiation by sampling the fluorescence and background signal levels at selectable but different time periods. The trigger signal used to synchronize the boxcar integrator with the laser was produced by directing a small fraction of the laser beam to a high-

speed photodiode (Tropel Inc., Fairport, NY) as shown in Figure 1. A tilted quartz plate was used as a beam splitter. In order to compensate for the inherent delay time in the boxcar gating circuits, a delay line was inserted between the PMT output and the boxcar integrator. This delay line was constructed from 22 m of RG58/U (50 Ω -impedance) coaxial cable, which was coiled and provided with proper shielding to minimize electromagnetic interference.

Three different systems were employed to record data processed by the boxcar integrator; the device chosen for a specific application was based on the required data storage and treatment. An analog strip-chart recorder (model 7100B, Hewlett-Packard, Palo Alto, CA) was used to measure most averaged fluorescence signals processed by the boxcar integrator. However, to record high resolution data for laser pulse characterization and fluorescence lifetime studies, the boxcar integrator was interfaced either directly to a digital computer (model 980A, Texas Instrument Co.) or to a digital paper tape punch (Models 251 and 622, Digitec, United Systems Co., Dayton, OH) for later processing. The choice between these two digital data collecting options was based both on availability of each device and complexity of the required data processing. Whichever device was selected, a parallel output channel was connected to the strip-chart recorder to enable data to be viewed continuously.

System Characterization

Burner and Flame Design. In order to avoid the distortions produced by pre- and post-filter effects in the fluorescence measurements, and to maximize

the detected fluorescence signal, a careful choice of the size of the flame and of the burner top was required. Three different burner head designs investigated in this study are shown in Figure 2. Each burner head consists of a nickel-plated brass cylinder 1.9 cm thick into which was drilled a given number of holes (.95 mm diameter), the configuration of which governed the size and shape of the flame.

Burner type A (cf. Figure 2) employed 192 holes arranged in 8 concentric circles. The six inner circles of burner ports support the flame gases, while the two outer rows are used for production of the flowing argon sheath. The resulting circular flame had an analytically useful diameter of 1.6 cm. Ultimately, burner top A was rejected because the flame which it produced exhibited marked post-filter effects. To avoid post-filter effects with this burner top, the position of the laser beam had to be changed from the center of the flame, for low analyte concentrations, to the edge of the flame (closer to the detector system) for increased analyte concentrations.

Burner head B (cf. Figure 2) was fabricated with five rows of fifteen holes each, arranged in a rectangle. The three inner rows supported the flame gases while the outer two rows carried the argon sheath. This burner top produced a rectangular flame of dimensions approximately 5 mm x 25 mm. This type of flame produced negligible post-filter effects when irradiated down its long dimension because approximately 85% of the total flame width can be illuminated by the laser beam. However, the rectangular flame, because of its large gas consumption, produces much more dilute atomic vapor compared to typical circular flames, and was consequently rejected for the bulk of work in this study.

Nonetheless, the rectangular flame was found useful in empirically determining the optimal flame configuration. Because the rectangular flame exhibited negligible post-filter effects, its small dimension was

felt to be satisfactory for further work. The optimum value for the flame long dimension (in line with the laser beam) would then be governed by the entrance angle of the viewing detection system and the distance between the flame and the detector. Thus, when the long axis of the flame fills the solid angle usable by the detection system (monochromator, in this case), any further increase in flame length would only increase the consumption of flame gases and decrease the usable fraction of generated atoms.

To determine the flame length usable by this detection system, the rectangular burner was positioned with its long axis in line with the laser beam and perpendicular to the direction in which fluorescence was detected. The amplitude of the fluorescence signal was then measured as the flame was moved past the monochromator entrance slit in a direction parallel to its long axis. This procedure causes the flame to subtend a progressively greater fraction of the entrance aperture, to produce an increasing fluorescence signal. Once the entrance angle has been completely filled, however, no further signal increase can occur. The distance between the flame position at which the signal first appears and that where it levels off therefore indicates the optimal flame length.

This optimal length was found to be 1 cm, so that the best flame cross-section would be 0.5 cm x 1 cm or, alternatively, a 1 cm circle. From this information, burner top C (cf. Figure 2) was designed. The three inner circular rows of burner ports support the flame gases, while the outer row is used for the argon sheath. The resulting circular flame has a diameter of 1.0 cm and a stable, analytically useful height between 15 to 20 cm, depending on the oxidant and fuel gases used.

Beam Characteristics and Radiation Collection. To maintain a uniformly illuminated flame volume, the diameter and power of the laser beam must be held constant and its homogeneity assured (33,34). Unfortunately, nitrogen-pumped dye lasers produce notoriously inhomogeneous beams, whose dimensions and radiant power can change with dye concentration, cavity alignment, and other factors. To improve beam homogeneity, consistency and quality within the flame atom cell, a quartz lens of 90 cm focal distance was used to defocus the laser beam and direct it to an aperture of 3.1 mm diameter (see Figure 3). The defocused, spatially limited beam was then allowed to pass through the observation region in the flame. To minimize divergence of the beam between the aperture and the flame, the aperture was placed at the shortest practical distance (8 cm) from the center of the flame.

To ascertain the dimensions of the final dye laser beam, the beam was attenuated and sent into a low sensitivity photographic emulsion (Panatomic-X, Kodak) which was located at the center of the burner top (corresponding to the center of the flame). An optical attenuator consisting of several layers of homogeneously exposed film was inserted in front of the photographic emulsion to avoid over-exposure and minimize the amount of acattered radiation in the emulsion which would otherwise distort the measured beam image.

The quality and homogeneity of the irradiance beam produced by this arrangement is indicated by the photographs in Figure 4, which are similar to those taken with Panatomic film for measuring beam dimensions, but were made using a high-contrast copy film to enhance the sensitivity of the measurement to beam homogeneity. In this figure, a ninefold magnification of the print portraying the actual size of the beam was made to increase visual sensitivity

of the effect. Figure 4A shows the dye laser output beam without any aperture in its path, while Figure 4B portrays the defocused, homogeneous beam that was finally employed.

Laser Pulse Characteristics. Because the present optical design (Figure 3) renders the spatial profile of the laser radiation nearly homogeneous across the illuminated region of the flame (cf. Figure 4), incident spectral power density could be calculated by knowledge of the beam peak power, the area being illuminated, and the spectral profile of the excitation beam.

Laser peak power was determined from the integrated laser energy incident on the flame and the temporal profile of the laser pulse. A fast pyroelectric joulemeter (Model J3-05 Molectron Co.) was employed to measure the laser energy incident on the flame. The output of the joulemeter, which was placed behind the flame in such a way that it intercepted the entire laser beam, was connected to a fast oscilloscope (Model 485, Tektronix Inc., Beaverton, OR). This combination not only provided a measure of incident laser energy, but indicated pulse-to-pulse fluctuations in the laser beam (± 8%), and revealed any progressive decrease in excitation power caused by degradation of the dye solution.

The temporal character of the exciting laser pulse, found to be critical in studies of saturation (28,32), was determined by scattering a small portion of the laser beam toward the detection system by means of an appropriately placed beam splitter. Obviously, if the time response of the detection system were a delta function, the output signal would represent the excitation pulse directly. However, under the experimental conditions of this study, this output signal is the time convolution of the laser pulse with the time response of the detection system.

Mathematically, this output signal is expressed by

$$i(t) = G(t) * L(t) \tag{1}$$

where

i(t) is the time-varying detected photoanode current representing the output (detected) pulse (scattered radiation).

G(t) is the instrument response function which, in this case, is the time-response of the photomultiplier tube/readout array;

L(t) is the time behavior of the excitation pulse or laser pulse

and

* represents the convolution operation.

The instrumental response function of the detection system can be approximated by the impulse response of the PMT, which is mathematically expressed by the Heaviside exponential:

$$G(t) = \begin{cases} C\, e^{-t/T} & t > 0 \\ 0 & t < 0 \end{cases} \tag{2}$$

where

T is the fall time of the photoanode pulse

and

C is a proportionality constant.

Now, assuming that the time profile of the laser pulse can be described by a Gaussian function, L(t) is given by

$$L(t) = L_o\, e^{-t^2/2\sigma^2} \qquad -\infty < t < +\infty \tag{3}$$

where

L_o is the maximum intensity of the laser pulse

and

σ is the standard deviation of the Gaussian pulse. The half width of the Gaussian function at half the maximum intensity ($t_{1/2}$), is then:

$$t_{1/2} = \sigma(\ell n 4)^{1/2} \tag{4}$$

By using the definition of the convolution integral, the expression for the output signal becomes

$$i(t) = \int_{-\infty}^{+\infty} G(t-t')\, L(t')\, dt' \tag{5}$$

Substitution of Eqs. (2) and (3) into Eq. (5) and integrating the resulting expression yields:

$$i(t) = \left(\frac{CL_o}{T}\right) e^{-t/T}\, e^{\sigma^2/2T^2} \left\{1 + \text{erf}\left[\frac{1}{\sqrt{2}}\left(\frac{t}{\sigma} - \frac{\sigma}{T}\right)\right]\right\} \tag{6}$$

By curve-fitting the experimental data to Eq. 6 one obtains values for σ and T which describe the excitation pulse and the instrumental re-

sponse. A typical curve-fit of the digitized output signal from the detection system (photomultiplier tube and boxcar integrator) to Eq. (6) is shown in Figure 5. In Figure 5, the experimental points are represented by squares and the solid curve is the best fit to those experimental points obtainable from Eq. (6). The values of the parameters σ and T which produced the best curve-fit are 2.36 ns and 3.6 ns respectively. This value of σ corresponds to a Gaussian pulse of width equal to 5.6 ns at half maximum. Any error in the measurement $i(t)$ is essentially given by the resolution or total rise time of the PMT and the response time of the boxcar integrator. The rise time of the PMT is approximately 1.2 ns (measured with a 250 ps rise-time sampling oscilloscope), the rise time of the sampling unit used in the boxcar integrator is $\sim$1 ns and the time-base jitter on the order of 100 ps. Consequently, the total rise time and, ultimately, the resolution of the above studies, corresponds to $\pm$ 1.5 ns.

The bandwidth of the exciting laser radiation was measured from the apparent excitation spectrum of the transition being studied. In turn, this excitation spectrum was obtained by slowly scanning the dye laser's output wavelength across the atomic line. The spectrum so obtained is obviously the convolution of the spectral profiles of the laser emission and the atomic absorption line. However, because the atomic lines used in this study were at least tenfold narrower than the spectral emission profile of the laser, the contribution of the atomic line to this measurement can be neglected. The bandwidth of the laser was therefore taken as the width at half height of the measured excitation spectrum. Throughout most of the

visible spectral region, an average value of 0.04 nm was obtained for the emission bandwidth of the laser beam. Because nearly the same bandwidth was measured regardless of the atomic transition being employed, the assumption that the atomic line contributes little to the half-width measurement seems well justified. Finally, the area of the exciting laser beam (0.076 cm^2) was ascertained from a photograph of the beam at the center of the flame (cf. Figure 4).

Initial Adjustments

To roughly set the boxcar integrator aperture (gate) delay, laser radiation is scattered toward the monochromator entrance slit from a glass plate placed above the burner top. The gate delay is then scanned by the boxcar integrator until a maximum signal is obtained.

Next, the flame is ignited and a high concentration (~100 µg/ml of the desired analyte solution is nebulized into it. With the laser irradiating the atoms so produced, and with the boxcar integrator gate delay optimized, the dye laser wavelength is accurately centered on the atomic transition by observing the generated fluorescence signal at the boxcar integrator output.

Because the time position of the maximum amplitude of the fluorescence signal depends on the fluorescence lifetime of the transition and not just on the laser pulse width, the temporal position of the sampling gate of the boxcar must next be re-adjusted to correspond to the fluorescence signal maximum. Finally, the dye laser wavelength is fine-tuned to ensure that it is centered on the desired excitation wavelength.

The foregoing alignment procedure is all performed using a relatively low laser power density so that a true maximum fluorescence signal, below the saturation level, is achieved.

Reagents and Chemicals

All the standard sample solutions used in this investigation were prepared from dried reagent-grade salts, which were dissolved in hydrochloric or nitric acids of analytical reagent grade (Mallinckrodt).

Determination of SSPD

In this study, the spectral power density required to saturate atomic transitions (SSPD) was determined from plots of spontaneous fluorescence signal as a function of incident radiant power. In these measurements, the spectral power density of the exciting beam was varied by inserting neutral density filters into it. The power density of the excitation beam could also have been varied by adjusting the driving power of the dye-pumping nitrogen laser. However, if this latter method of power control is employed, care must be taken to ensure that the size and spatial homogeneity of the dye laser beam do not change. In all measurements, the neutral density filters were placed exactly perpendicular to the beam, ensuring that the position or the optical and spatial characteristics of the beam in the flame are not altered between measurements.

Because the duration of the laser system employed in this study is 5.6 ns and the spontaneous fluorescence lifetimes of atomic transitions are of the same order of magnitude (35), a non-steady-state population of the excited atomic energy level should prevail. Therefore, for atomic transitions involving only two energy levels, the following equation (26) was used to curve-fit the experimental data:

$$\bar{n}_2 = n_0 B_{12} \left(\frac{\rho_0}{a_2 + b_2 \rho_0} \right) (1 - D) \qquad (7)$$

where

$$D = \frac{1}{(a_2 + b_2 \rho_0) t_0} \left(1 - e^{-(a_2 + b_2 \rho_0) t_0} \right) \qquad (8)$$

and $\bar{n}_2$ (cm^{-3}) is the average density of atoms in excited energy level 2 during the excitation pulse (the magnitude of the detected fluorescence signal is proportional to $\bar{n}_2$); n_0 (cm^{-3}) is the total atomic density, which is assumed to be distributed among the two energy levels involved; t_o is the duration (half-width) of the excitation pulse; ρ_0(W/cm^2Hz) is the peak spectral power density of the laser pulse, B_{12} is the Einstein coefficient for the stimulated absorption transition 1→2; $a_2 = A_{21} + Z_{21}$, where $A_{21}(s^{-1})$ is the Einstein coefficient for spontaneous emission between levels 2 and 1, and $Z_{21}(s^{-1})$ is the rate of collisional deactivation; $b_2 = B_{12} + B_{21}$, where B_{21} ($\frac{cm^2 \cdot Hz}{W \cdot sec}$) is the Einstein coefficient for the radiationally induced downward transition 2→1.

In equation (7) the curve fit parameters are the intensity of the fluorescence signal and the a and b lumped variables. Experimentally, the non-steady-state SSPD (ρ_s^{NSS}) was defined as the incident spectral power density required to produce an upper level population just half of that required for saturation. Ideally, a complete saturation is achieved when incident spectral power density approaches infinity. Under those conditions the population of the excited energy level becomes (cf. Eqs. 7-8).

$$(\bar{n}_2)sat = n_0 \frac{B_{12}}{b_2} \qquad (9)$$

Using the procedure described above, saturation curves were measured for a number of transitions of several elements, and under various experimental conditions which should affect the measured values. Specifically, the effects of experimental variables such as the aperture gatewidth of the detector, the flame composition, the analyte concentration and the spectral characteristics of the transitions were investigated.

RESULTS AND DISCUSSION

Effect of Detector Aperture

The excitation pulse used in these experiments has an approximately Gaussian shape of 5.6 ns half-width (cf. Fig. 5), rather than the square pulse shape assumed in the model presented in Part I of this study (26). Therefore, it is important to evaluate which time during the excitation process is best for determining the excited-state population (i.e. for sampling the generated fluorescence).

A square excitation pulse, of the kind assumed (26), will contain approximately the same energy as that in a Gaussian pulse of the same amplitude and of half-width equal to the duration of the square pulse. Therefore, to obtain an experimental measurement of the upper state population which corresponds most closely to the theoretical model (26), it would seem most reasonable to probe the fluorescence generated by the excited atoms at a time corresponding to the peak of the Gaussian laser pulse (32). However, because any real measurement system must sample the fluorescence for a finite time interval, it must be expected that some error will be introduced during such sampling by the portion of the sampled interval during which the exci-

tation pulse power has fallen substantially below its peak value (32). The importance of this error was evaluated here by measuring the atomic fluorescence produced at various incident laser power levels as a function of the detector gate width.

Saturation plots for the manganese $^6S_{5/2}$ - $^6P_{5/2}$ transition at 403.3 nm, shown in Fig. 6, were obtained with detection gatewidths of 1 ns and 5 ns, selected merely on the basis of instrumental capability. From Figure 6, it is apparent that twice the power density is required to produce apparent saturation for the signal detected with the 5 ns gatewidth than when the 1 ns gatewidth is used. Clearly, because the 1 ns gatewidth more closely samples the atomic fluorescence during the peak of the excitation pulse, it provides a measure of the upper state population which more exactly matches the assumed model (26) and will produce a more accurate value for SSPD. Because the 1 ns gate is already substantially smaller than the 5.6 ns (FWHM) laser pulse, it can be assumed that little improvement in accuracy would be obtained through use of a shorter gatewidth. This assumption was validated by means of measurements taken with a sampling oscilloscope of 250 ps gate width.

Although more accurate SSPD values can be obtained by use of a 1 ns detection gate than a 5 ns gate, several practical considerations dictate that the longer gate width be employed for many experimental measurements.

The reason it is experimentally more difficult to employ a 1 ns gate than a 5 ns gate revolves around dye laser long-term drift and stability, and the necessity of taking measurements over long time periods. In general, the time position of the maximum of an atomic fluorescence peak (where measurements for saturation should ideally be taken) is determined by

the time convolution of the excitation pulse and the fluorescence lifetime of the transition (cf. Figure 5). However, the fluorescence lifetime of an atomic transition changes with the excitation power density, especially at high power densities where saturation of the excited energy level is approached. Therefore, a continuous change of the time position of the fluorescence peak occurs along measurements taken for a saturation curve. Of course, an accurate determination of the peak fluorescence can be obtained by time-scanning a narrow detector gate over the fluorescence signal for each value of excitation power density. However, under such conditions, the measurement of saturation curves becomes a very long and tedious procedure (approximately 20 hours per curve). With this scanning procedure, one would obviously need to change dye solutions between measurements, in order to avoid degradation of the dye during the series; in turn, dye replacement requires realignment of the dye cell in the laser cavity with each change of solution. To avoid those problems, a 5 ns gatewidth was employed in most of the following experimental measurements.

Because the time envelope of the laser pulse does not change appreciably with wavelength (i.e. with the transition under observation) and because the lifetimes of atoms examined in this study fall within a relatively narrow range, the factor-of-two difference between real SSPD's and those measured with a 5 ns gate is likely to be maintained. This statement is strengthened by a comparison of the SSPD's obtained for Na at 589.0 nm, which also exhibit a twofold difference between the values obtained with a 5 ns and 1 ns gate width. In all measurements to be reported later, a detection gate width of 5 ns was used unless otherwise stated; in all these cases, a more accurate SSPD value will probably be obtained by division of the cited value by a factor near 2.

Let us now discuss the effects of the concentration of analyte atoms in the flame, the composition of the flame and the spectral characteristics of the excitation source on the measured SSPD values.

Effect of Analyte Concentration

According to the theoretical analysis in Part I of this study (26), the concentration of absorbing species (analyte atoms in the flame) determines the magnitude of an observed fluorescence signal, but should not appreciably affect the power density required to saturate the excited energy level. This expected result is experimentally verified for the $^1S_o \rightarrow {}^1P_1$ transition of Ca (422.7 nm) by Figure 7. Figure 7 shows the experimental saturation curves (adjusted to fit on the same scale) for 10 ppm and 1,000 ppm Ca in an air-acetylene flame. One can see that within experimental error, the same saturation power density of 1.1×10^{-7} W/cm^{2}Hz is obtained in both cases.

Effect of Flame Composition

Ideally, variations in composition of an atom cell should affect only rates of collisionally induced atomic transitions and ionization (32); the importance of such collisions to the saturation of atomic transitions could then be verified experimentally and compared with the theoretical model proposed (26). However, alteration of the environment of an atom reservoir such as a flame changes not only the collisional quenching and ionization rates of excited atoms but also the efficiency of atom production and, consequently, the total population of atoms available within the flame.

Fortunately, as experimentally proven above, the concentration of analyte atoms does not appreciably affect the measured saturation power density. Therefore, any change in flame composition which affects SSPD can be attributed almost entirely to quenching or ionization.

The effect on SSPD of fuel-to-oxidant ratio in an air-acetylene flame was examined for the Ca 422.7 nm transition. For lean, stoichiometric, and fuel-rich flames, SSPD values of 1.16×10^{-7}, 1.14×10^{-7}, and 1.10×10^{-7} W/cm^{2}Hz were measured, respectively, indicating that neither atomization efficiency nor flame temperature strongly affect saturation. Interestingly, ionization of excited-state species, which can distort saturation curves when longer laser pulses are employed (32), seems not to be a factor in our studies. Presumably, the influence of ionization is reduced because of the brief excitation pulse being used here, and the finite time required for collisional ionization to occur.

The effect of flame composition on SSPD is further examined in Figure 8, which shows the 377.5 nm transition of Tl being saturated in the different flame environments described in Table I. In curves A and B, acetylene was used as fuel gas, while in curves C and D, hydrogen was the fuel gas. Also, the nitrogen diluent in the air used as an oxidant gas in the flames used for curves A and C was replaced by argon in curves B and D to study the quenching effects of nitrogen. Nitrogen has been assumed to be one of the main quenchers in air-supported flames. The saturation power densities obtained in these different flame environments are 4.4×10^{-8}, 6.1×10^{-8}, 3.0×10^{-8}, and 2.7×10^{-8} W/cm^{2}Hz, respectively. The same small variations in SSPD with flame composition were observed in the case of Sr at 460.7 nm,

as a resonance transition. In this latter case, the values of SSPD for the A, B and C flames were 5.5×10^{-8}, 5.8×10^{-8}, and 5.3×10^{-8} W/cm^{2}Hz, respectively. These differences are not deemed to be significant for these particular measurements and the accuracy of the curve-fitting program.

Effect of Atomic Properties of the Elements on Energy Level Saturation

Let us now consider, for a given element and atomic environment, how saturation affects transitions of different kinds and at different wavelengths. Specifically, an attempt was made to investigate differences in saturation characteristics between two lines of Tl and two of In. In both cases, the two lines were at different wavelengths and involved both resonance and non-resonance transitions.

A partial term diagram illustrating the transitions of In at 410.1 and 451.1 nm is given in Figure 9 (35). Experimental values for SSPD of the 410.1 nm and 451.1 nm transitions were 8.5×10^{-8} and 6.0×10^{-8} W/cm^{2}Hz, respectively. The ratio of the saturation power densities of the two transitions $\frac{\rho_s(451.1)}{\rho_s(410.1)}$ is 0.7 a figure which can be compared to that which would be predicted by the theory presented in Part I of this study (26).

Assuming that the transitions $2 \rightarrow 3$ and $2 \rightarrow 1$ (Figure 9) are the primary deactivation paths of an excited atom in level 2, the effects of saturation on those transitions can be explained by using the three-energy-level model described previously (26). Because the energy separation between levels 3 and 1 (0.274 eV), is similar to the thermal energy of

the flame (kT = 0.198 eV) one can assume a thermal equilibrium between those levels. Thus, under steady-state excitation (long-term irradiation) of level 2, the saturation power densities of the transitions considered are given from Eqs. 39, 36 and 37 of Part I of this study (26) by:

$$\rho_s^{ss}\ (410.1\ \text{nm}) = \frac{(A_{21} + Z_{21} + A_{23} + Z_{23})}{B_{21}\left(1 + \frac{g_2/g_1}{(1+Z)}\right)} \tag{10}$$

and

$$\rho_s^{ss}(451.1\ \text{nm}) = \frac{(A_{23} + Z_{23} + A_{21} + Z_{21})}{B_{23}\left(1 + \frac{g_2/g_3}{(1+Z^{-1})}\right)} \tag{11}$$

where, $Z = \frac{Z_{13}}{A_{31} + Z_{31}}$; A_{21}, A_{23} are the Einstein coefficients for the spontaneous emission from level 2 to 1 or level 2 to 3 respectively; A_{31} is the Einstein coefficient for the spontaneous transition from level 3 to level 1; $Z_{21}(s^{-1})$, $Z_{23}(s^{-1})$ are the rates of collisional deactivation of the excited atom in level 2 to levels 1 and 3 respectively; $Z_{13}(s^{-1})$ is the rate of collisional activation of atoms from level 1 to level 3; $B_{21}(W/cm^2Hz)^{-1}$, $B_{23}(W/cm^2Hz)^{-1}$ are the Einstein coefficients for the radiationally induced transitions of the excited atoms in level 2 to levels 1 and 3 respectively; and g_1, g_2 and g_3 are the degeneracies of energy levels 1, 2 and 3, respectively. Therefore, the ratio of the theoretical SSPD's of the 451.1 nm line and the 410.1 nm line is:

$$\frac{\rho_s^{ss}(451.1\ \text{nm})}{\rho_s^{ss}(410.1\ \text{nm})} = \frac{B_{21}}{B_{23}} \frac{\left(1 + \frac{g_2/g_1}{(1+Z)}\right)}{\left(1 + \frac{g_2/g_3}{(1+Z^{-1})}\right)} \tag{12}$$

By substitution of the relationship between the A and B coefficients the above expression becomes:

$$\frac{\rho_{\varepsilon}^{ss}(\lambda 51.1\ nm)}{\rho_{\varepsilon}^{ss}(\lambda 10.1\ \mu)} = \frac{A_{21}}{A_{23}} \left(\frac{\lambda_{21}}{\lambda_{23}}\right)^3 \frac{\left(1 + \frac{g_2/g_1}{(1+Z)}\right)}{\left(1 + \frac{g_2/g_3}{(1+Z^{-1})}\right)} \tag{13}$$

Assuming $A_{31} \ll A_{21}$, the parameter Z becomes

$$Z \simeq \frac{Z_{13}}{Z_{31}} = (g_3/g_1)\exp\left(-\frac{(E_3 - E_1)}{kT}\right) \tag{14}$$

Then, by substitution of $E_3 - E_1 = 0.274$ ev and an average value of 2300° K for the temperature of the flame, one obtains

$$Z \simeq 0.5$$

From Eq. (13), in order to calculate the ratio of the saturation power densities, one needs the values of the Einstein coefficients A_{21} and A_{23}. Those coefficients can be calculated from their relationship to the respective oscillator strengths (55):

$$A_{ij} = \frac{8\pi^2 e^2}{m_e c} \frac{f_{ij}}{\lambda^2_{ij}} \tag{15}$$

where m_e and e are the mass and the charge of one electron, respectively, c is the speed of light, and f_{ij} is the oscillator strength for the transition $i \rightarrow j$. The values of the A_{ij} coefficients calculated with Eq. (15) and the parameters used in those calculations are given in Table III. From these values and an assumed collision rate

ten (10x) times higher than the rate of spontaneous emission, a ratio of the saturation power densities of 0.84 results. Thus, the calculated value for the ratio of the saturation power densities is only 17 percent higher than that obtained experimentally; the remaining disparity can be ascribed to assumptions made in the foregoing treatment. Of the assumptions which probably introduce some error, the most important are those involving the Z variable, the rate of quenching collisional deactivation and the assumption of steady-state irradiation of the excited levels. In ascribing a value of the Z parameter, we have assumed a negligible contribution from spontaneous emission; in the values for collisional quenching rates, we have assumed a value equal to ten (10x) times the respective rate of spontaneous emission.

Effect of Resonance and Non-Resonance Transitions.

An attempt was made to determine the effect of saturation on non-resonance transitions of both the stepwise and direct-line type and to compare this behavior with that observed for resonance transitions. Of these, direct-line fluorescence was found to be the most practically important.

In the study of direct-line fluorescence, the $^2P_{1/2} \rightarrow {}^2S_{1/2}$ and $^2P_{3/2} \rightarrow {}^2S_{1/2}$ transitions of Tl (377.5 nm and 535.0 nm) were employed. A partial term diagram of these transitions is displayed in Figure 10. Experimentally, the atoms were excited with 377.5 nm laser radiation and both the resonance fluorescence at 377.5 nm and the non-resonance direct-line fluorescence at 535.0 nm were detected. Saturation curves obtained for these transitions in a hydrogen-air flame are shown in Figure 11.

The experimental SSPD values for the 377.5 nm and 535.0 nm lines are 3.0×10^{-8} W/cm^2 Hz and 2.8×10^{-8} W/cm^{2}Hz, respectively. Because the

excited level 2 is involved in both transitions and the excitation process arises only through absorption at a single wavelength (377.5 nm), this similarity is not surprising; the observed 7 percent difference is found to be within experimental error.

Another interesting system to study is a non-resonance stepwise fluorescence process where the excitation and de-excitation processes involve different excited energy levels. An example of such a measurement would be the detection of the 589.6 nm line of Na following excitation of the Na-atoms with radiation at 589.0 nm. However, this latter case would not have any practical application nor fundamental importance because both lines have comparable sensitivities as resonance transitions, are in the same wavelength region, and have already been found to be in extremely rapid equilibrium (32,36).

Comparison of Experimental and Predicted Values of Saturation Power Density.

Experimentally measured and predicted SSPD values for several atomic transitions are compared in Table IV. The experimental values of the saturation power density were obtained from saturation curves of the listed transition in an air-acetylene flame. These experimental data were curve-fitted with the theoretical equation pertaining to each particular kind of transition. In every case but Tl (measured in an air/H_2 instead of air/C_2H_2 flame), the rate of quenching collisions (Z) has been assumed to

be 25 times the corresponding rate of spontaneous emission (A). This value is justified on the basis of recent measurements in our laboratory (29). None of the experimental values were corrected for the approximate factor-of-two error caused by use of a 5 ns rather than 1 ns detection gate width. Importantly, the theoretical SSPD values are a factor of 4π larger than predicted by our earlier model (26) because of an error in the definition of the Einstein B coefficient which was used (40).

Considering the factor-of-two probably error, close agreement can be seen between the experimental and the predicted values of saturation power density for most transitions. Only the values for Na and Mn lack this close agreement.

For the transition of Mn (403.3 nm) there is a factor of 11 difference between the experimental and predicted results. Such a difference and the extremely high experimental value of saturation power density are believed due to the existence of other deactivation pathways than the ones considered in the two-level model which was employed here. The Mn "level" to which excitation occurred is actually a triplet and cannot be adequately treated with this simple model. Moreover, to properly consider a four-level model would require a knowledge or assumption of the quenching rates among the three upper levels and the ground level. Lack of this information would negate the advantages of such an extensive treatment.

For the Na 589.0 nm transition (Table IV) a surprising factor of 12 exists between the predicted and experimental SSPD values. Again, the error is thought to be caused by the inability of the model (26) to deal with atoms having multiplet excited states. Because of this difficulty, the value cited

in Table IV is taken from a steady-state (long-term irradiation) model (32), which does not correspond exactly to the conditions of this study.

Also listed in Table IV are several SSPD values obtained from a model for steady-state saturation (26), expected for irradiation by a laser pulse which is long compared to the lifetime of the excited state. As mentioned above, this steady-state treatment is the only one applicable to some transitions because of limitations in the transient model (26) and the lack of availability of non-radiative transition rates. For those transitions (Ca, Sr, Mn) for which both treatments could be used, predicted differences between the models are small, and would in most cases be obscured by observation errors. The reason for these small differences is the relatively rapid quenching (25 times the natural radiative deactivation rate) which has been assumed here and observed (39) in the air/C_2H_2 flame. Because of this rapid quenching, true excited-state lifetimes are short (< 1 ns), making the steady-state model applicable.

CONCLUSIONS

In this paper, experimental SSPD values for a number of atomic transitions occurring in air-acetylene and H_2/air flames were measured and compared with theoretical values predicted by a published model (26). In characterizing the "saturation" of atomic energy levels, the effects of the analyte concentration and the nature of the atom-environment on the saturation power density of several resonance and non-resonance atomic transitions were explored. For this latter investigation, flames having different compositions and temperatures were used as atom-cells.

These studies have shown that the source power necessary to saturate an atomic level does not depend significantly on the analyte atom concentration or on the atom's environment. However, factors which strongly affect the SSPD are the wavelength of radiation used to excite the atoms, the rates of the different deactivation paths of the transition being studied, and the degeneracy of the two energy levels involved in the excitation path. These findings suggest that the saturation power density is just a property of the transition studied and is relatively independent of the atomizer used.

As expected, for atomic systems involving three or more excited energy levels, agreement between the experimental SSPD values and those predicted by the theoretical three-energy level model (26) is not good. As the number of additional atomic energy levels involved in the investigated system increases, the number of possible deactivation pathways also increases, necessitating the introduction of simplifying assumptions and consequent inaccuracies into the non-steady-state treatment. Also, in most analytically useful flames (e.g. air/C_2H_2; N_2O/C_2H_2), non-radiative deactivation rates are sufficiently fast that the non-steady-state model (26) need not be applied. However, for even shorter pulses, such as those produced by synchronously pumped dye lasers (39), use of the transient model should be necessary.

ACKNOWLEDGEMENT

Taken in part from the Ph.D. thesis of D. Rojas de Olivares, Indiana University, 1976. Supported in part by the National Science Foundation through grants CHE 77-22152 and CHE 79-18073 and by the Office of Naval Research.

REFERENCES

1. Wood, R. W., Phil. Mag. 10, 513 (1905).
2. Wood, R. W., Phil. Mag. 23, 689 (1912).
3. Winefordner, J. D., and Vickers, T. J., Anal. Chem. 36, 161 (1964).
4. Winefordner, J. D., and Staab, R. A., Anal. Chem. 36, 165 (1964).
5. Winefordner, J. D., and Staab, R. A., Anal. Chem. 36, 1367 (1964).
6. Jenkins, D. R., Spectrochim. Acta, Part B, 23, 167 (1967).
7. Massmann, H., Spectrochim. Acta, Part B, 23, 215 (1968).
8. West, T. S. and X. K. Williams, Anal. Chim. Acta 45, 27 (1969).
9. Sullivan, J. V. and Walsh, A., Spectrochim. Acta 21, 721 (1965).
10. Dagnall, R. M., and West, T. S., Appl. Opt. 7, 1287 (1968).
11. Zacha, K. E., Bratzel, M. P., Winefordner, J. D. and Mansfield, J. M., Anal. Chem. 40, 1733 (1968).
12. Piepmeier, E. H., Spectrochim. Acta, Part B, 27, 431 (1972).
13. Piepmeier, E. H., Spectrochim. Acta, Part B, 27, 445 (1972).
14. Omenetto, N., Benetti, P., Hart, L., Winefordner, J. D. and Alkemade, C. Th. J., Spectrochim. Acta, Part B, 28, 289 (1973).
15. Omenetto, N., Hart, L. P., Benetti, P. and Winefordner, J. D., Spectrochim. Acta, Part B, 28, 301 (1973).
16. Kuhl, J. and Spitschan, H., Opt. Comm. 7, 256 (1973).
17. Kuhl, J., Neuman, S. and Kriese, M., Z. Naturforsch. 28A, 273 (1973).
18. Neuman, S. and Kriese, M., Spectrochim. Acta, Part B, 29, 127 (1974).
19. Hercher, M., Appl. Opt. 6, 947 (1967).
20. Bolshov, M. A., Zybin, A. V., Zybina, L. A., Koloshnikov, V. G., Majorov, I. A., Spectrochim. Acta, Part B, 31, 493 (1976).

21. Hohimer, J. P., Hargis, P. J., Jr., Appl. Phys. Lett. 30, 344 (1977).

22. Boutilier, G. D., Blackburn, M. B., Mermet, J. M., Weeks, S. J., Haraguchi, H., Winefordner, J. D., Omenetto, N., Appl. Opt. 17, 2291 (1978).

23. Sharp, B. L., Goldwasser, A., Spectrochim. Acta, Part B, 31, 431 (1976).

24. Smith, P , Winefordner, J. D., Omenetto, N., J. Appl. Phys. 48, 2676 (1977).

25. Daily, J. W., Chan, C., Combust. Flame 33, 47 (1978).

26. Olivares, D. and Hieftje, G. M., Spectrochim. Acta, Part B, 33, 79 (1978).

27. Omenetto, N., Hart, L. P. and Winefordner, J D., Appl. Spectrosc. 26, 612 (1972).

28. Rojas de Olivares, D., Ph.D. Thesis, Indiana University, 1976.

29. Hollander, T., Ph.D. Thesis, University of Utrecht, The Netherlands, (1964).

30. Hieftje, G. M., Ph.D. Thesis, University of Illinois, (1969).

31. Hieftje, G. M. and Bystroff, R. I., Spectrochim. Acta, Part B, 30, 187 (1975).

32. Van Calcar, R. A., Van de Ven, M. J. M., Van Uitert, B. K., Biewenga, K. J., Hollander, Tj., and Alkemade, C. Th. J., J. Quant. Spectrosc. Radiat. Transfer 21, 11 (1979).

33. Rodrigo, A. B. and Measures, R. M., IEEE J. Quantum Electron. QE-9, 972 (1973).

34. Daily, J. W., Appl. Opt. 17, 225 (1978).

35. Mavrodineanu, R. and Boiteux, H., "Flame Spectroscopy", Wiley, New York, NY (1965).

36. Chen, H. L., and Fried, S., IEEE J. Quantum Elec. QEII, 669 (1975).

37. Gaydon, A. G. and Wolfhard, H. G., "Flames, Their Structure, Radiation and Temperature", Chapman and Hall, London, (1970).

38. Smyly, D. S., Townsend, W. P., Zeegers, P. J. Th. and Winefordner, J. D., Spectrochim. Acta, Part B, 26, 53 (1971).

39. Russo, R. E., Indiana University, Personal Communication, 1980.

40. Mitchell, A. C. G., and Zemansky, M. W., Resonance Radiation and Excited Atoms, Cambridge Press, N.Y., 1971, p. 95.

GLOSSARY

$a_2 = A_{21} + Z_{21}$ = for 2-level atomic model (26)

$b_2 = B_{12} + B_{21}$ = for 2-level atomic model (26)

a_{3S}, b_{3S}, c_{3S} = lumped parameters pertaining to direct-line fluorescence from a 3-level atomic model in which the lower level involved in the transition is assumed to have a steady-state population. (26)

A_{ji} = Einstein coefficient for spontaneous emission from level j to level i (s^{-1})

c = speed of light (3×10^{10}cm/s)

D = departure of rate-controlled <u>average</u> population of excited level (under non-steady-state irradiation) from the population produced by steady-state irradiation. (19)

E_i = Energy of atomic level i

g_i = degeneracy (statistical wieght) of the ith energy level

h = Planck's constant = 6.624×10^{-34} J-s

k = Boltzmann constant

λ_{ji} = wavelength corresponding to a transition from energy level j to energy level i (nm)

n_0 = total atomic density in <u>all</u> levels under consideration

$\overline{n_j} = \overline{n_j(t)}$ - average atomic density in upper level j during the excitation pulse

$(n_j)_{sat}$ = population density of level j under conditions of complete saturation

ν_{ji} = spectral frequency corresponding to a transition from level j to level i

ρ_0 = peak spectral power density of exciting radiation (W/cm^2Hz)

$\rho_s = \frac{a_2}{b_2}$ = saturation spectral power density for 2-level atomic model

t = time

t_0 = excitation pulse length

T = absolute temperature (°K)

τ = natural (spontaneous) lifetime for transition of interest = $1/A_{21}$

τ' = observed fluorescence lifetime for transition of interest = $1/a_2$

$Z = Z_{13}/a_{31}$ (see Eq. 9)

Z_{ij} = rate of collisional (radiationless) transition from level i to level j (s^{-1})

Table 1. Flame Characteristics*

Flame Type	Supply Gases Fuel	Oxidant	Flows (ℓ/min)	Temperature (K)	Ref.
A	C_2H_2		2.5	2300	(35)
		Air	18.8		
B	C_2H_2		2.5	2600	(37)
		O_2	4.7		
		Ar	14.3		
C	H_2		16.2	1800	(35)
		Air	18.8		
D	H_2		16.2	2200	(38)
		O_2	4.7		
		Ar	14.3		

*In all flames, an argon shield (6 ℓ/min) was used.

Table II. Effect of flame composition on the SSPD of the $^2P_{3/2} \rightarrow {}^2S_{1/2}$ transition of Tl (377.5 nm).

Flame Composition	ρ_s (W/cm^2 Hz) x 10^8
C_2H_2/Air	4.4
C_2H_2/O_2 - A_r	6.1
H_2/Air	3.0
H_2/O_2 - A_r	2.7

Table III. Values of atomic parameters of the 410.1 nm and 451.1 nm transitions of In. λ is the wavelength of the transition studied; g_i and g_j are the statistical weights of the upper and lower energy levels of the transition; f is the oscillator strength and A is the Einstein coefficient for spontaneous emission (35).

Transition	λ(nm)	g_i/g_j	f	A x 10^8(s^{-1})
$^2P_{1/2} \rightarrow {}^2S_{1/2}$	410.1	1	0.235	0.932
$^2P_{3/2} \rightarrow {}^2S_{1/2}$	451.1	0.5	0.33	2.16

Table IV. Experimental and Predicted values of Saturation Spectral Power Densities (SSPD)

Element	λ(nm)	Theoretical SSPD (Non-steady-state model) (W/cm^2 Hz) x 10^8	Theoretical SSPD (Steady-state model) (W/cm^2 Hz) x 10^8	Experimental SSPD (W/cm^2 Hz) x 10^8	Saturation Power Density (W/cm^2) x 10^{-3}[a]
Na[d]	589.0		4.8	62	8.4
Ca	422.7	4.3	4.3	11	1.8
Sr	460.7	3.4	3.3	5.5	0.79
Mn[e]	403.3	5.9	5.0	66	12
In[c]	410.1		23	8.5	1.5
In[c]	451.1		19	6.0	0.88
Tl[c,d]	377.5		2.5	3.0	0.63
Tl[b,c,d]	535.0		2.5	2.8	0.29

[a] Saturation power density required from a laser of bandwidth 0.01 nm.

[b] This transition was studied as a direct line fluorescence process. The excitation wavelength was 377.6 nm and the fluorescence signal was detected at 535.0 nm.

[c] Steady-state three-energy-level model (26) was used to calculate ρ_s.

[d] Measured in air/H_2 flame; rate of quenching collisions (Z_{21}) assumed to be 10 times A_{21}.

[e] Because of the small energy difference between the energy levels $P_{3/2}$, $P_{5/2}$, and $P_{7/2}$ of Mn, the triplet was treated as a single energy level with a degeneracy equal to the sum of those of the three levels (namely $g_2' = 18$). A two-energy-level model (steady state and non-steady state) (26) was then employed to calculate ρ_s.

Figure Legends

Figure 1. Block diagram of the laser-excited atomic fluorescence apparatus; FD, frequency doubler; D, photodiode; F, flame; PM, photomultiplier.

Figure 2. Top view of burner-port configurations. Dimensions given in cm. Port diameters were 0.95 mm in all cases.

Figure 3. Schematic diagram of the optical system. All distances are in cm. The focal length (f) of the lens used to defocus and direct the dye laser beam into the flame was 90 cm. The distance X between the dye laser output and the center of the flame was 300 cm or 50 cm for atomic transitions with wavelengths corresponding to the visible or ultraviolet spectral regions, respectively. This change in distance was required to obtain the highest possible radiant flux of the ultraviolet radiation, whose magnitude is reduced over that of the visible laser radiation because of the inefficiency of frequency doubling.

Figure 4. Magnified photograph of laser beam spatial profile at the center of flame.

A. Magnified (9X) print of the original dye laser output.

B. Magnified (9X) print of the spatially homogeneous beam used in the present study. See text for discussion.

Figure 5. Time profile of the laser pulse (excitation wavelength = 403.3 nm). The experimental data (□) were curve-fitted to the expression involving the convolution of the laser

pulse with the time response of the detection system (cf. Eq. (7)).

Figure 6. Saturation curves for Mn at 403.3 nm. Curves A and B correspond to detector gatewidths of 1 ns and 5 ns, respectively. Measured saturation power densities from these plots are: Curve A- 0.35 $\mu W/cm^2Hz$

Curve B- 0.65 $\mu W/cm^2Hz$

Experimental points represented by triangles (curve A) and squares (curve B); solid curves represent best fit of equation 7 to experimental points. To convert ρ_s from units of W/cm^2Hz to $W/cm^2 \cdot nm$, multiply by c/λ^2, where $c = 3 \times 10^{17}$ nm/s and λ is the wavelength (in nm) of the transition under consideration.

Figure 7. Effect of the concentration of analyte atoms on the saturation power density. Curves A and B correspond to concentrations of 10 ppm and 1,000 ppm of $CaCl_2$, respectively. The saturation power density in both cases was found to be 0.11 $\mu W/cm^2Hz$. Data represented by triangles (curve A) and squares (curve B); solid lines represent best fit of equation 7 to experimental points.

Figure 8. Flame composition effect on the saturation power density. Curves A, B, C and D correspond to acetylene-air, acetylene/oxygen-argon, hydrogen-air and hydrogen/oxygen-argon flames respectively. See Table I for

flame conditions. Solid lines represent the best fit of equation 7 to experimental points.

Figure 9. Partial term diagram of In. Both transitions indicated in the diagram were studied via resonance fluorescence.

Figure 10. Partial term diagram of Tl, showing resonance and non-resonance transitions which were investigated experimentally.

A. Resonance fluorescnece, detected at 377.5 nm;

B. Direct-line fluorescence, observed at 535.0 nm; and

C. Excitation (absorption) transition at 377.5 nm.

Figure 11. Saturation curves of resonance and non-resonance transitions of Tl in an air-hydrogen flame. Curve A corresponds to the resonance transition at 377.5 nm while curve B pertains to the direct-line fluorescence at 535.0 nm. See Figure 11 for particular transitions involved. Excitation of both transitions was accomplished by means of absorption of laser radiation at 377.5 nm. Measured saturation power densities from these plots are:

Curve A- 0.030 $\mu W/cm^2 Hz$

Curve B- 0.028 $\mu W/cm^2 Hz$

Experimental values (triangles and squares) curve fit to equation 8 to generate solid lines.

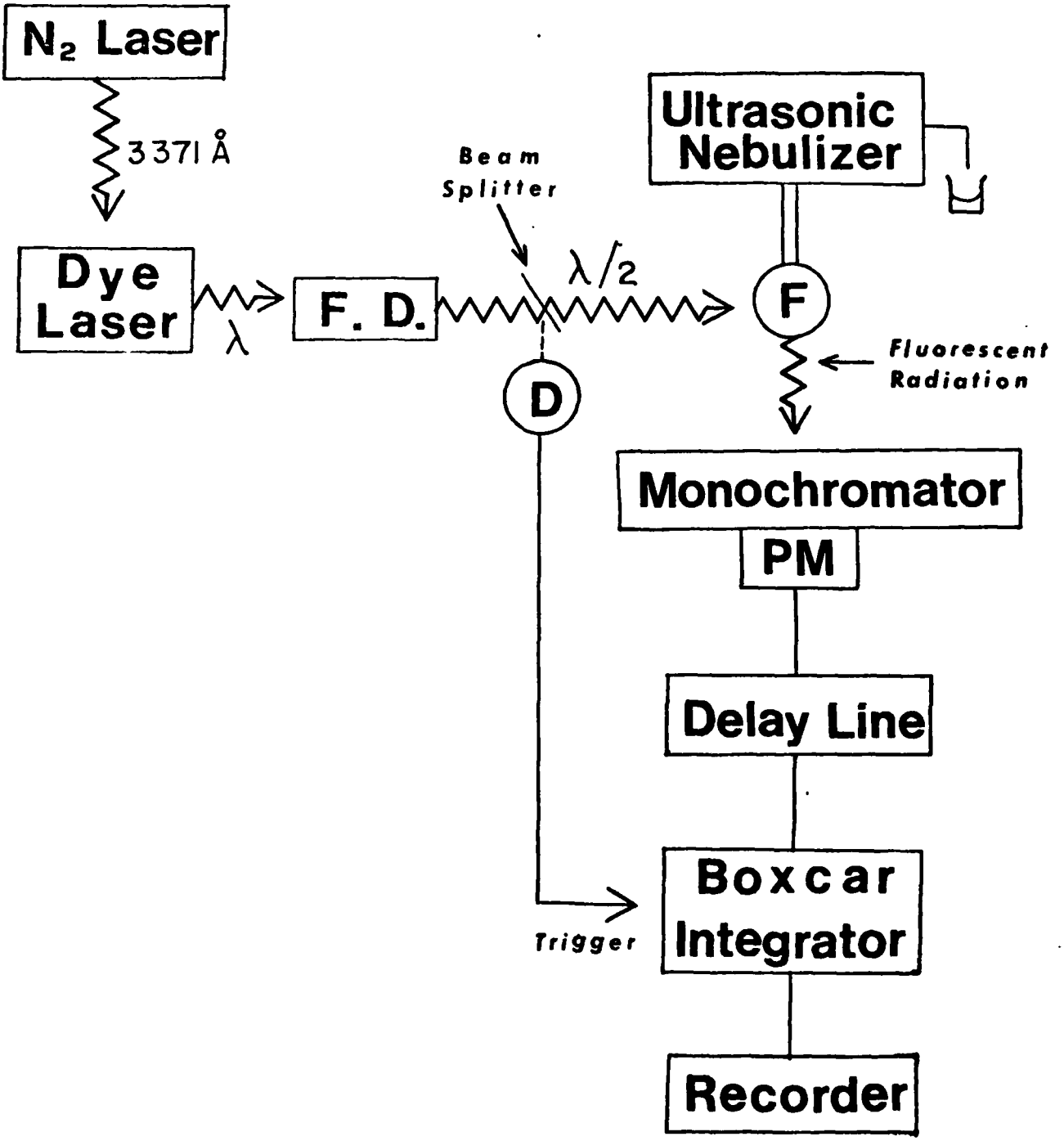
N_2 Laser
3371 Å
Dye Laser
λ
F. D.
Beam Splitter
λ/2
D
F
Ultrasonic Nebulizer
Fluorescent Radiation
Monochromator
PM
Delay Line
Boxcar Integrator
Trigger
Recorder

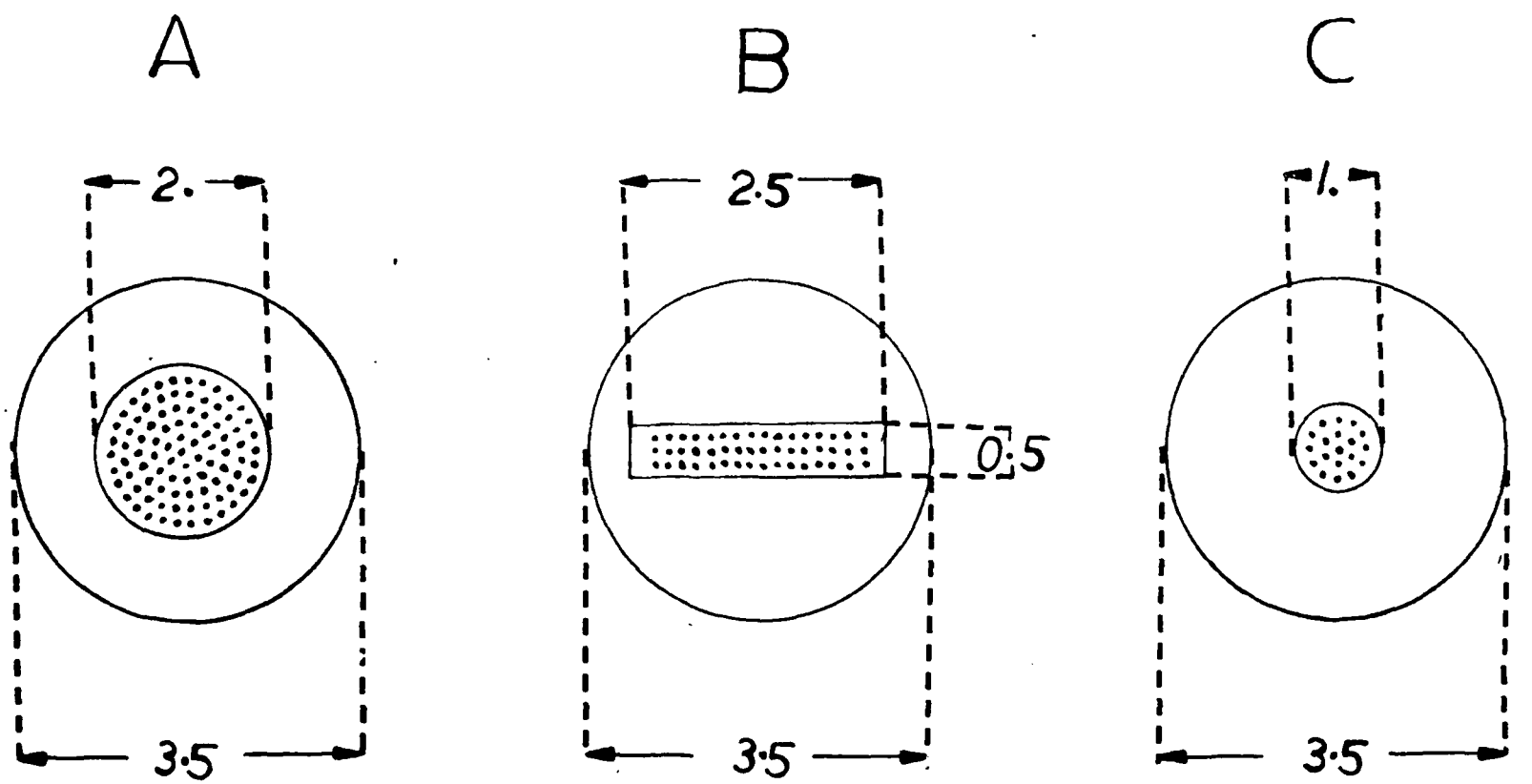
A
2.
3.5
B
2.5
0.5
3.5
C
1.
3.5

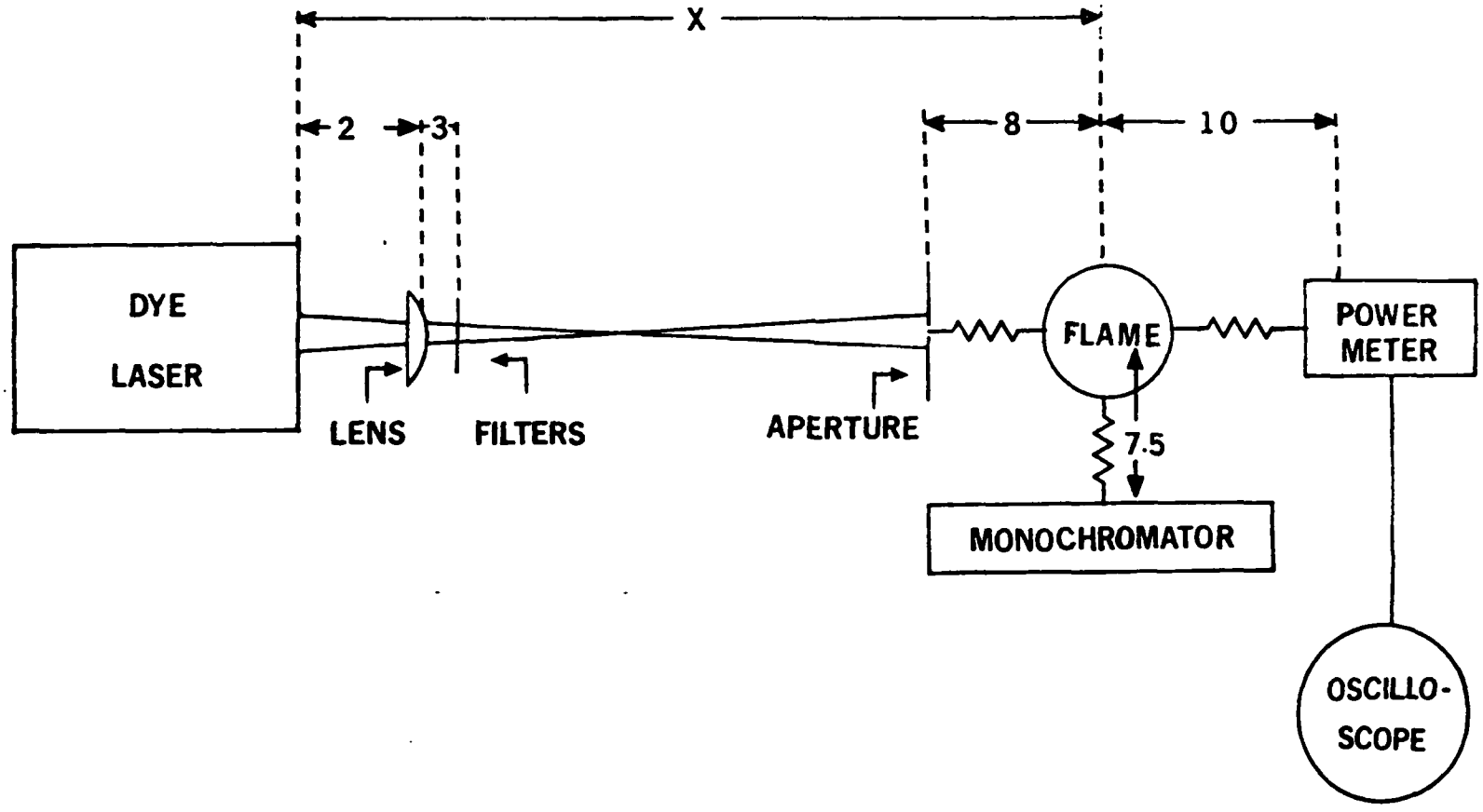
X
2
3
8
10
DYE
LASER
LENS
FILTERS
APERTURE
FLAME
POWER
METER
7.5
MONOCHROMATOR
OSCILLO-
SCOPE

A

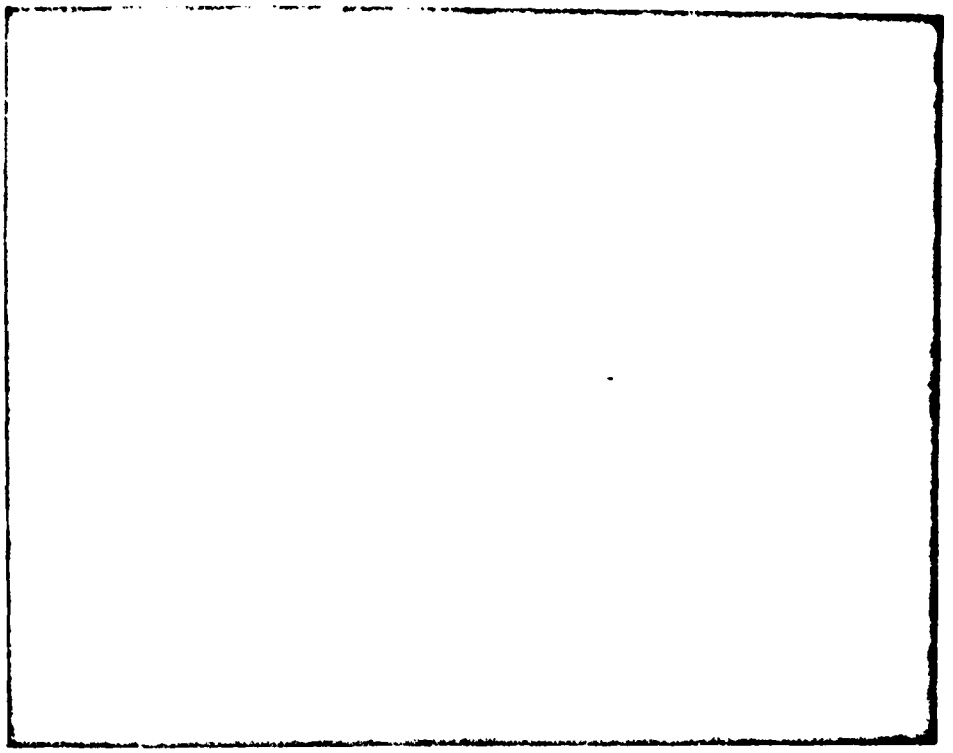

B

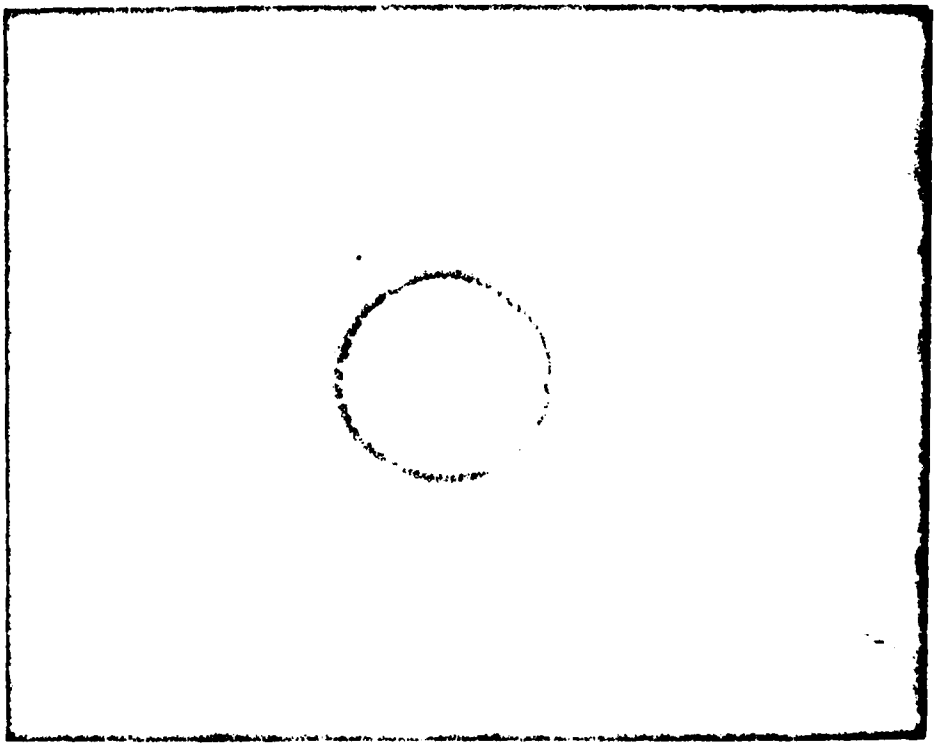

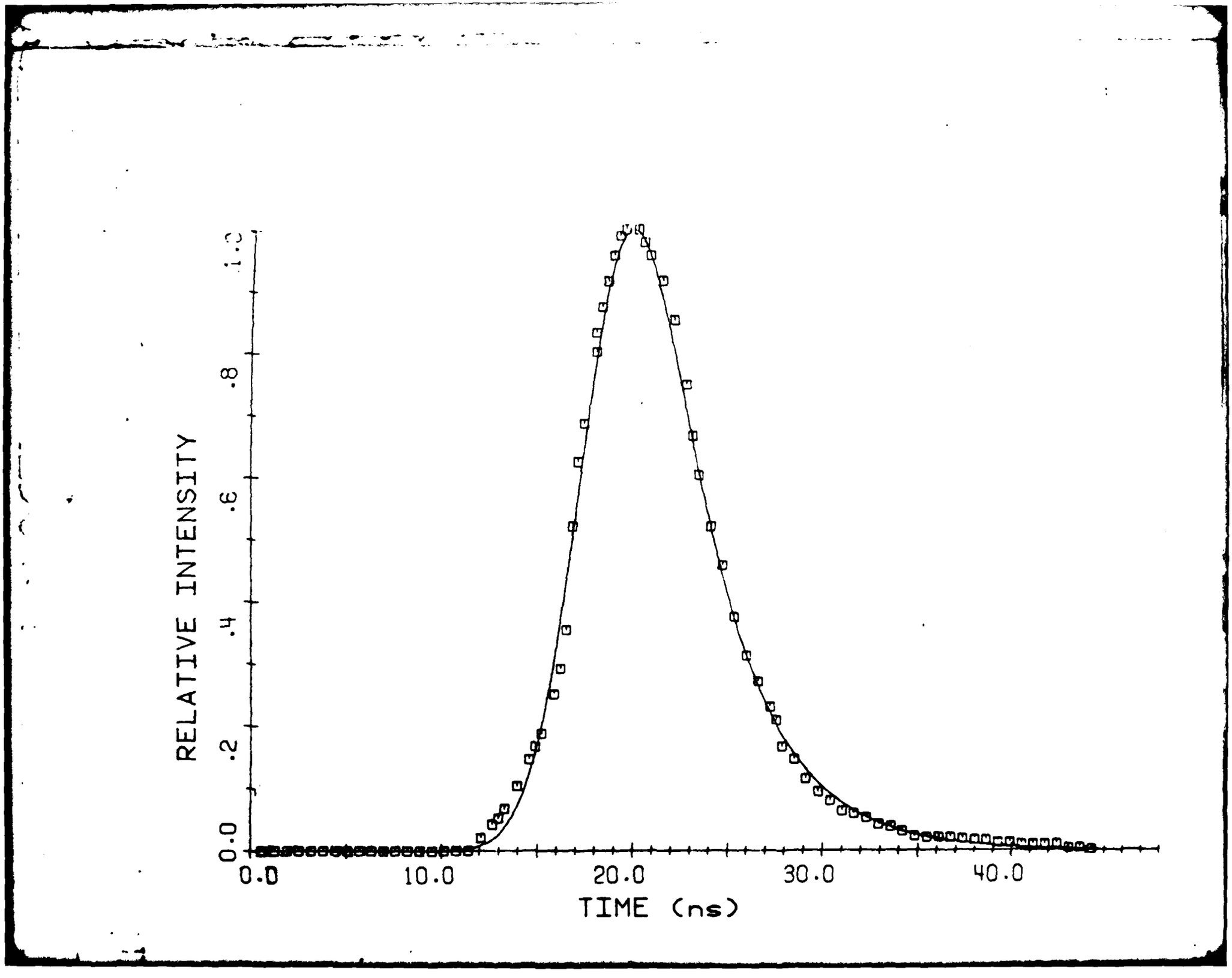
RELATIVE INTENSITY
0.0
.2
.4
.6
.8
1.0
0.0
10.0
20.0
30.0
40.0
TIME (ns)

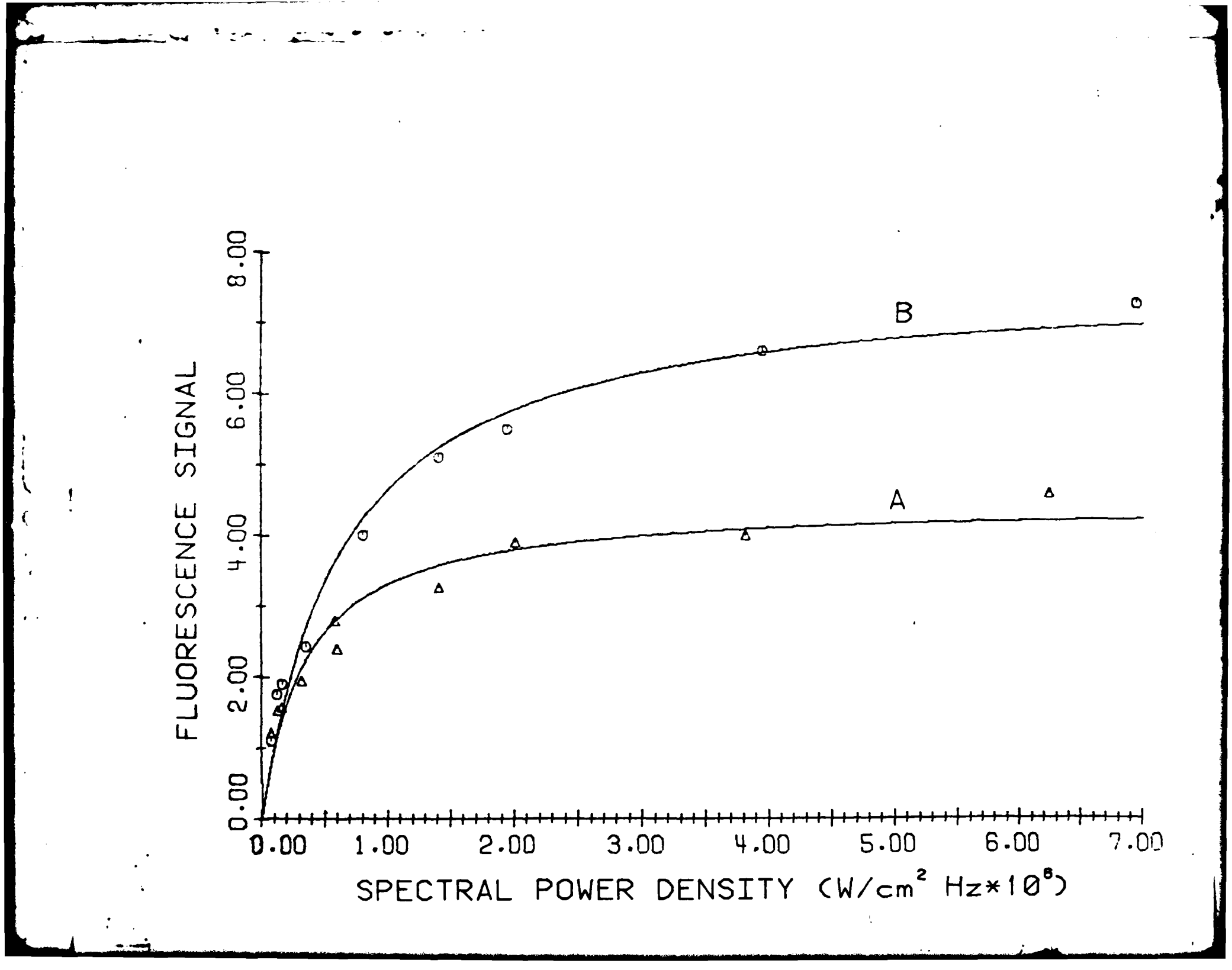
FLUORESCENCE SIGNAL
0.00
2.00
4.00
6.00
8.00
B
A
0.00
1.00
2.00
3.00
4.00
5.00
6.00
7.00
SPECTRAL POWER DENSITY (W/cm² Hz*10⁶)

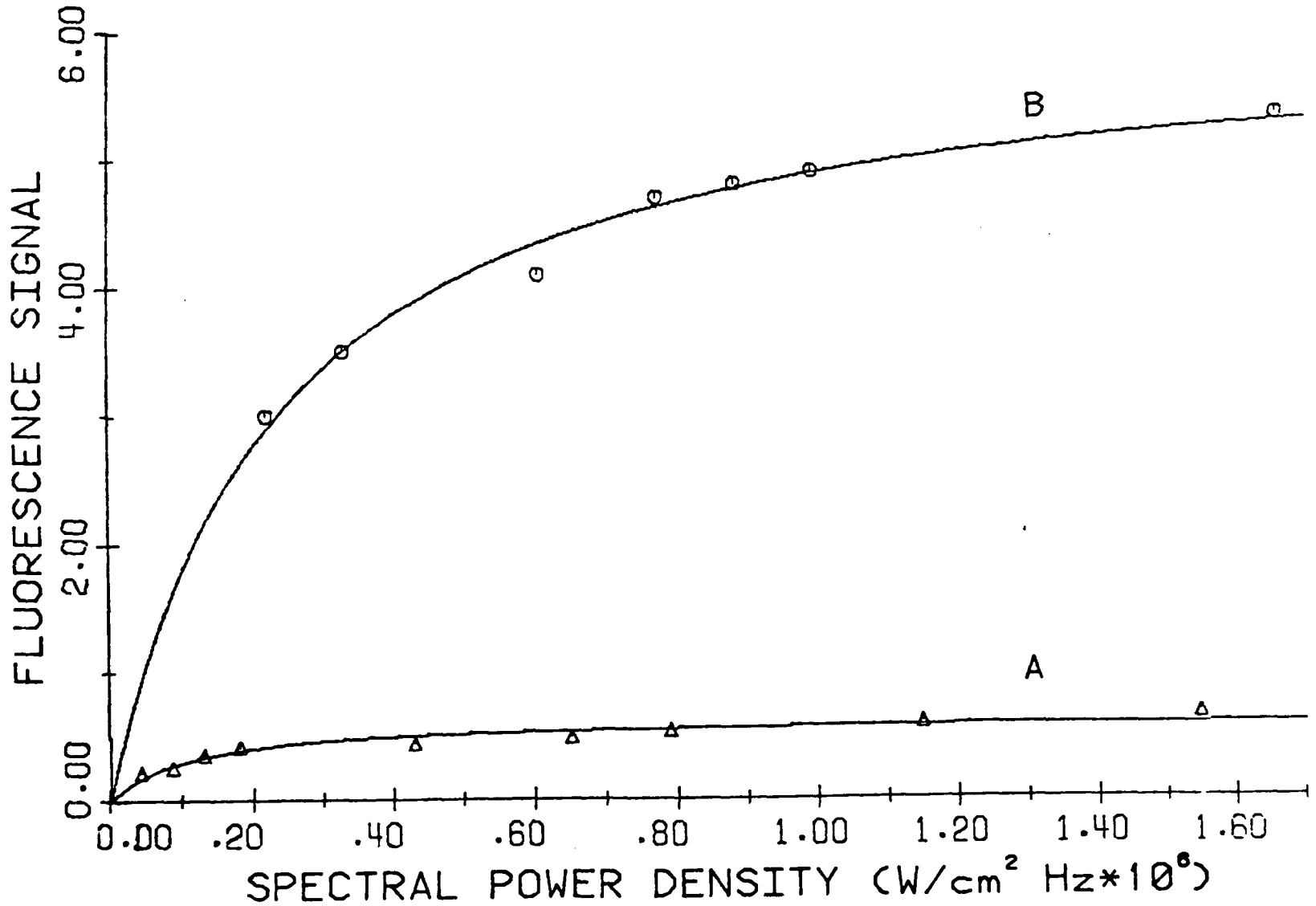
FLUORESCENCE SIGNAL
6.00
4.00
2.00
0.00
B
A
0.00
.20
.40
.60
.80
1.00
1.20
1.40
1.60
SPECTRAL POWER DENSITY (W/cm² Hz*10⁶)

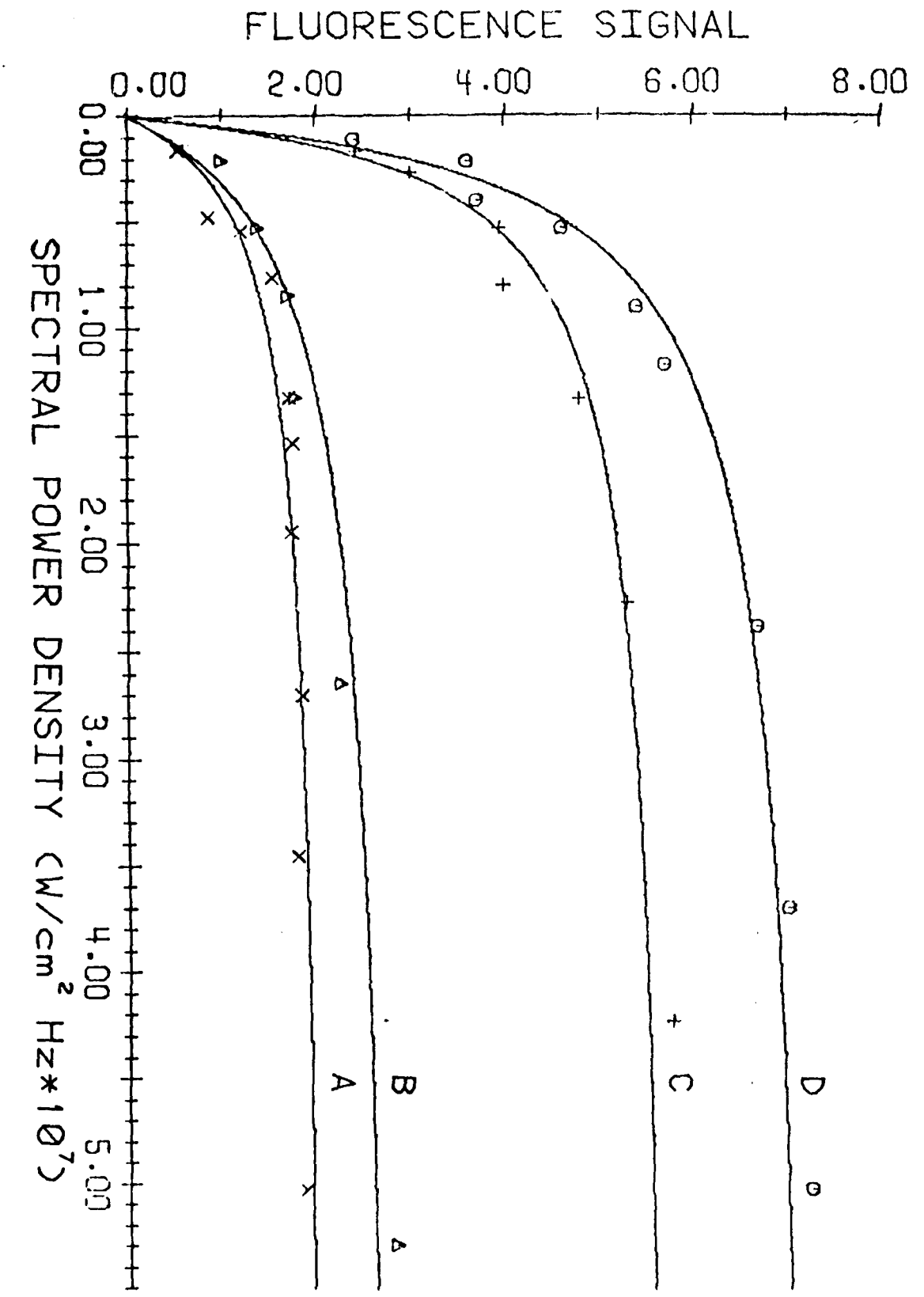
FLUORESCENCE SIGNAL
0.00
2.00
4.00
6.00
8.00
SPECTRAL POWER DENSITY (W/cm² Hz*10⁷)
0.00
1.00
2.00
3.00
4.00
5.00
A
B
C
D

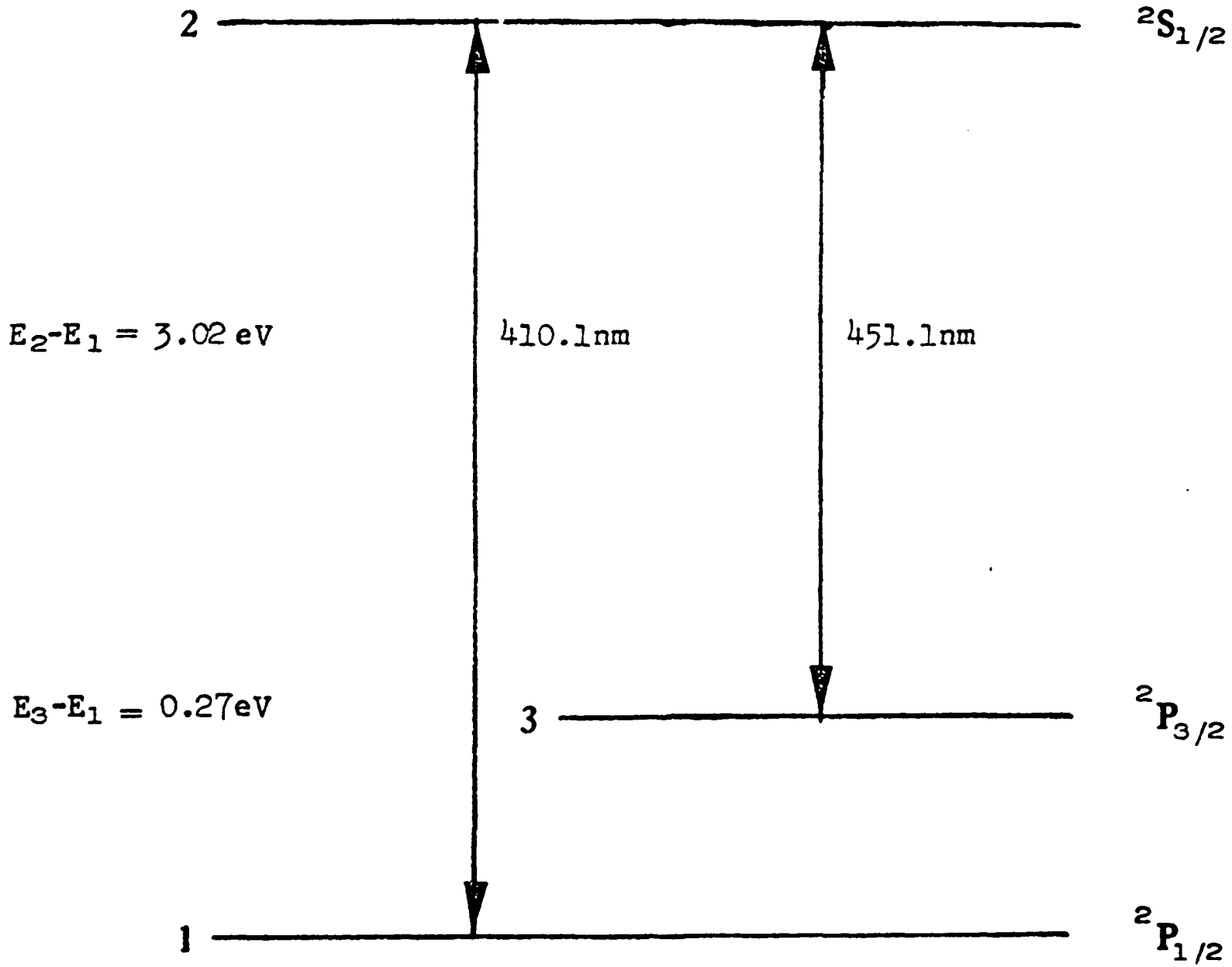
2
$^2S_{1/2}$
$E_2-E_1 = 3.02$ eV
410.1nm
451.1nm
$E_3-E_1 = 0.27$eV
3
$^2P_{3/2}$
1
$^2P_{1/2}$

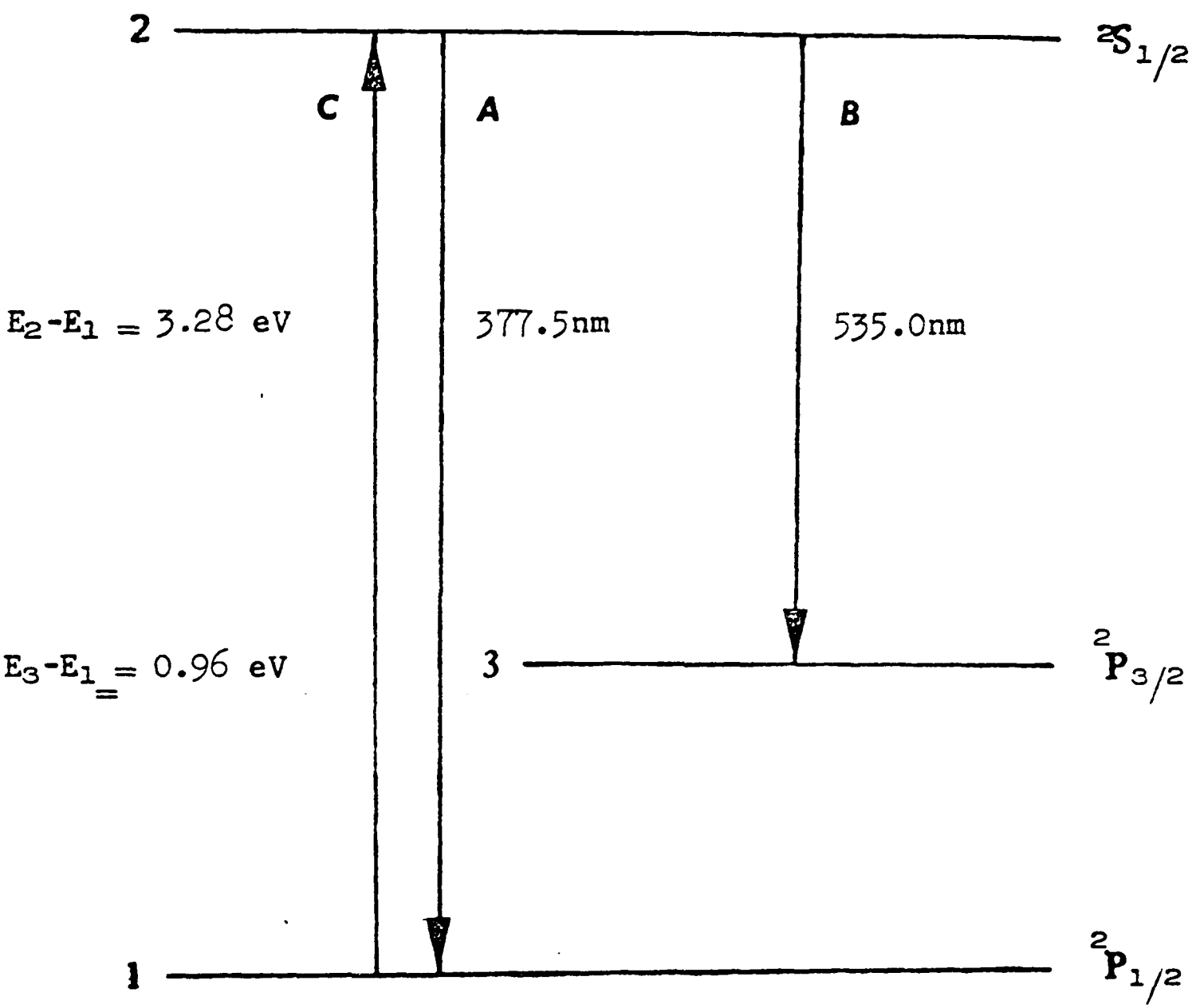
2
$^2S_{1/2}$
C
A
B
$E_2-E_1 = 3.28$ eV
377.5nm
535.0nm
$E_3-E_1 = 0.96$ eV
3
$^2P_{3/2}$
1
$^2P_{1/2}$

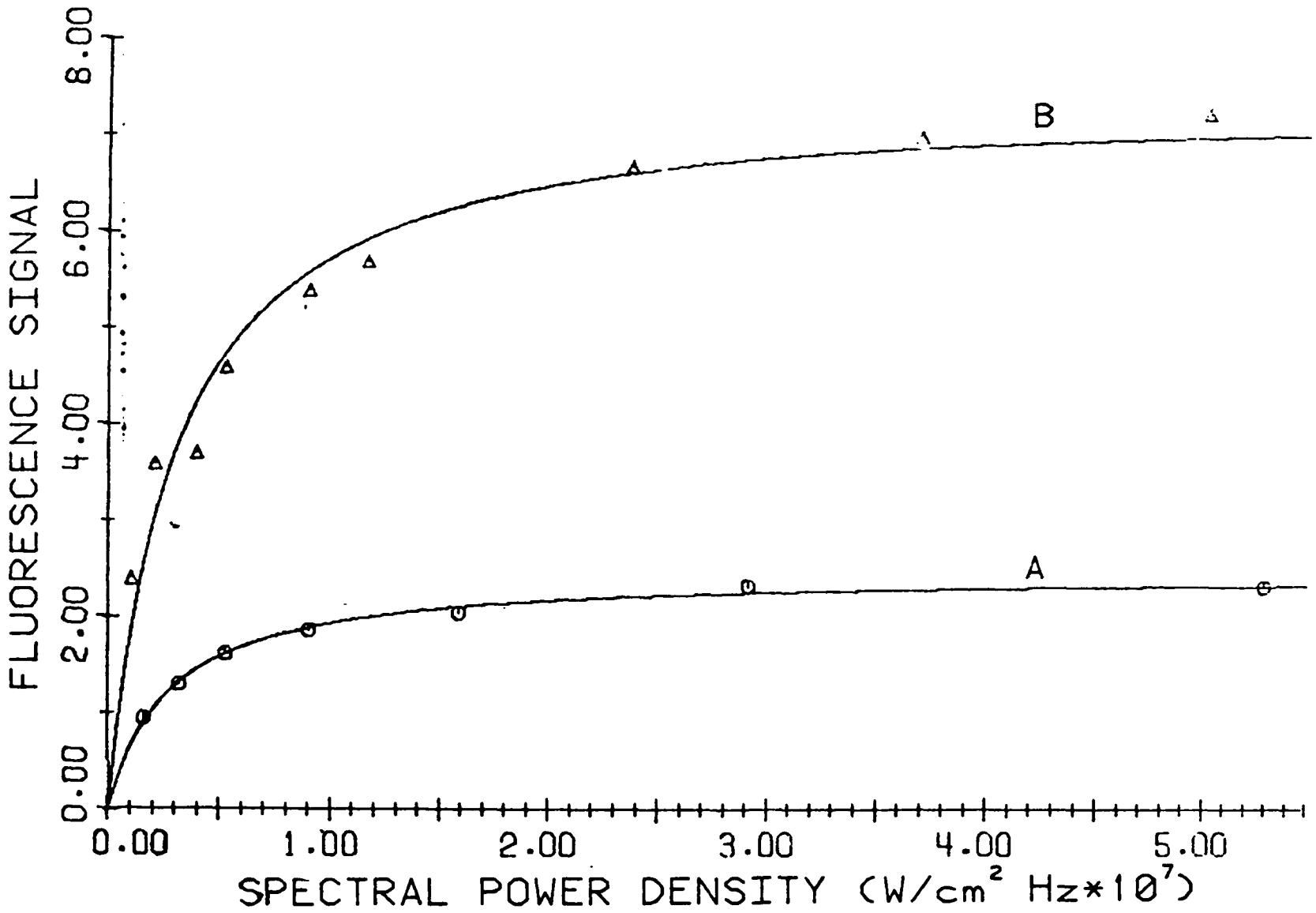
FLUORESCENCE SIGNAL
0.00
2.00
4.00
6.00
8.00
B
A
0.00
1.00
2.00
3.00
4.00
5.00
SPECTRAL POWER DENSITY (W/cm² Hz*10⁷)

SP472-3/B1

472:GAN:716:ddc
78u472-608

TECHNICAL REPORT DISTRIBUTION LIST, 051C

	No. Copies
Dr. M. B. Denton Department of Chemistry University of Arizona Tucson, Arizona 85721	1
Dr. R. A. Osteryoung Department of Chemistry State University of New York at Buffalo Buffalo, New York 14214	1
Dr. B. R. Kowalski Department of Chemistry University of Washington Seattle, Washington 98105	1
Dr. S. P. Perone Department of Chemistry Purdue University Lafayette, Indiana 47907	1
Dr. D. L. Venezky Naval Research Laboratory Code 6130 Washington, D.C. 20375	1
Dr. H. Freiser Department of Chemistry University of Arizona Tuscon, Arizona 85721	
Dr. Fred Saalfeld Naval Research Laboratory Code 6110 Washington, D.C. 20375	1
Dr. H. Chernoff Department of Mathematics Massachusetts Institute of Technology Cambridge, Massachusetts 02139	1
Dr. K. Wilson Department of Chemistry University of California, San Diego La Jolla, California	1
Dr. A. Zirino Naval Undersea Center San Diego, California 92132	1

	No. Copies
Dr. John Duffin United States Naval Postgraduate School Monterey, California 93940	1
Dr. G. M. Hieftje Department of Chemistry Indiana University Bloomington, Indiana 47401	1
Dr. Victor L. Rehn Naval Weapons Center Code 3813 China Lake, California 93555	1
Dr. Christie G. Enke Michigan State University Department of Chemistry East Lansing, Michigan 48824	1
Dr. Kent Eisentraut, MBT Air Force Materials Laboratory Wright-Patterson AFB, Ohio 45433	1
Walter G. Cox, Code 3632 Naval Underwater Systems Center Building 148 Newport, Rhode Island 02840	1
Professor Isiah M. Warner Texas A&M University Department of Chemistry College Station, Texas 77840	1
Professor George H. Morrison Cornell University Department of Chemisty Ithaca, New York 14853	1
Dr. Rudolph J. Marcus Office of Naval Research Scientific Liaison Group American Embassy APO San Francisco 96503	1
Mr. James Kelley DTNSRDC Code 2803 Annapolis, Maryland 21402	1

TECHNICAL REPORT DISTRIBUTION LIST, GEN

	No. Copies
Office of Naval Research Attn: Code 472 800 North Quincy Street Arlington, Virginia 22217	2
ONR Branch Office Attn: Dr. George Sandoz 536 S. Clark Street Chicago, Illinois 60605	1
ONR Area Office Attn: Scientific Dept. 715 Broadway New York, New York 10003	1
ONR Western Regional Office 1030 East Green Street Pasadena, California 91106	1
ONR Eastern/Central Regional Office Attn: Dr. L. H. Peebles Building 114, Section D 666 Summer Street Boston, Massachusetts 02210	1
Director, Naval Research Laboratory Attn: Code 6100 Washington, D.C. 20390	1
The Assistant Secretary of the Navy (RE&S) Department of the Navy Room 4E736, Pentagon Washington, D.C. 20350	1
Commander, Naval Air Systems Command Attn: Code 310C (H. Rosenwasser) Department of the Navy Washington, D.C. 20360	1
Defense Technical Information Center Building 5, Cameron Station Alexandria, Virginia 22314	12
Dr. Fred Saalfeld Chemistry Division, Code 6100 Naval Research Laboratory Washington, D.C. 20375	1
U.S. Army Research Office Attn: CRD-AA-IP P.O. Box 1211 Research Triangle Park, N.C. 27709	1
Naval Ocean Systems Center Attn: Mr. Joe McCartney San Diego, California 92152	1
Naval Weapons Center Attn: Dr. A. B. Amster, Chemistry Division China Lake, California 93555	1
Naval Civil Engineering Laboratory Attn: Dr. R. W. Drisko Port Hueneme, California 93401	1
Department of Physics & Chemistry Naval Postgraduate School Monterey, California 93940	1
Dr. A. L. Slafkosky Scientific Advisor Commandant of the Marine Corps (Code RD-1) Washington, D.C. 20380	1
Office of Naval Research Attn: Dr. Richard S. Miller 800 N. Quincy Street Arlington, Virginia 22217	1
Naval Ship Research and Development Center Attn: Dr. G. Bosmajian, Applied Chemistry Division Annapolis, Maryland 21401	1
Naval Ocean Systems Center Attn: Dr. S. Yamamoto, Marine Sciences Division San Diego, California 91232	1
Mr. John Boyle Materials Branch Naval Ship Engineering Center Philadelphia, Pennsylvania 19112	1

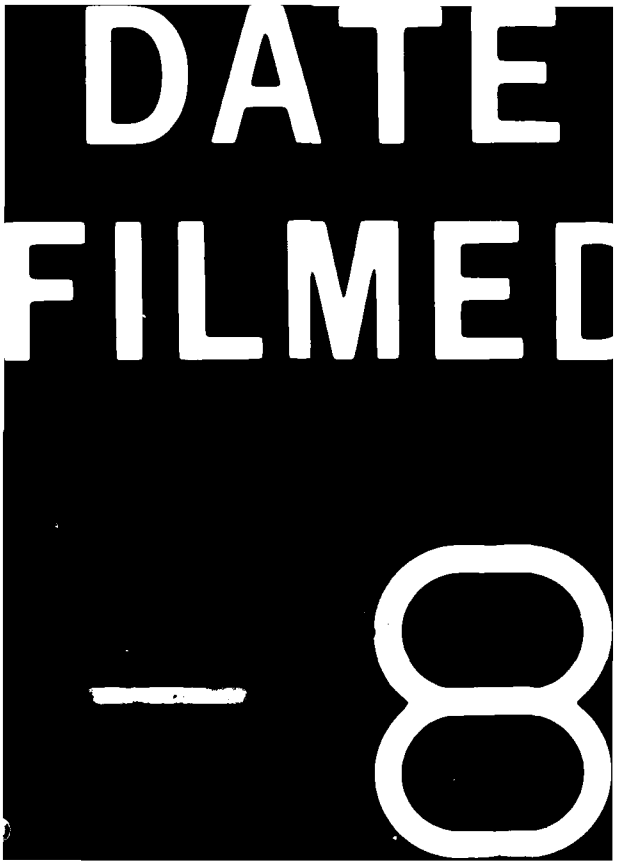
DATE
FILMED
8